A Systematic Study of ULF Waves Above F_{H^+} From GEOS 1 and 2 Measurements and Their Relationships With Proton Ring Distributions

SYLVAINE PERRAUT, ALAIN ROUX, PATRICK ROBERT, AND ROGER GENDRIN

Centre de Recherches en Physique de l'Environnement, Centre National d'Etudes des Télécommunications 92131 Issy-les-Moulineaux, France

JEAN-ANDRÉ SAUVAUD AND JEAN-MICHEL BOSQUED

Centre d'Etude Spatiale du Rayonnement, Centre National de la Recherches Scientifique Université Paul Sabatier, 31029 Toulouse Cedex, France

GERHARD KREMSER AND AXEL KORTH

Max-Planck-Institut für Aeronomie, D-3411 Katlenburg-Lindau 3, Federal Republic of Germany

A detailed analysis of the ULF noise observed on the GEOS magnetic antennas in the frequency range $\sim 0.2-12$ Hz has revealed the properties of structured emissions occurring just above the proton gyrofrequency whose existence was reported by Russell et al. (1970) and Gurnett (1976). These waves are observed in the vicinity of the geomagnetic equator at all L values between \sim 4 and \sim 8. They propagate in a direction perpendicular to the dc magnetic field. The waves consist of harmonically related monochromatic emissions. The fundamental frequency is generally of the order of the local proton gyrofrequency. Sometimes the fundamental and first harmonics are missing. If there is more than one fundamental frequency present, nonlinear coupling often occurs between the different emissions. The amplitudes of individual events vary from some tens of milligammas to some hundreds. Their duration ranges from some tens of minutes to some hours. Within the range of sensitivity of the detectors $(10^{-2} \text{ y Hz}^{-1/2} \text{ at 1 Hz}, 10^{-3} \text{ y Hz}^{-1/2} \text{ at 8 Hz})$ the average probability of emission occurrence during a given hour is 12%, this number increases to ~30% during the afternoon and in the premidnight sectors. Simultaneous observations of proton fluxes, as obtained from the two GEOS particle experiments show that these waves are often associated with distribution functions peaking at some energy (5 \leq E \leq 30 keV) for 90° pitch angle particles. This ring-like distribution provides the energy source for the excitation of non-resonant $(k_{\parallel} = 0)$ instabilities near nF_{H^+} (n = running number). A theoretical model is presented that qualitatively explains the main characteristics of the observed

1. Introduction

The magnetic equator is more and more recognized as being a region where specific phenomena occur. Besides of the fact that this is the region where plasma sheet particles are injected [Winckler, 1970; Mauk and McIlwain, 1974], where drift shell splitting and/or convection effects induce anomalous pitch angle and/or energy distributions [Ashour-Abdalla and Cowley, 1974; Roederer and Hones, 1974; Smith and Hoffman, 1974; Kivelson and Southwood, 1975; Konradi et al., 1973; Solomon, 1976] and where thermal heavy ions are concentrated [Young, 1979], it is also the region where most of the recently discovered waves have been found to be localized. This is true in the whole frequency range from below the ion frequency range up to the electron plasma frequency and above.

Contrary to classical whistler mode waves and to ion cyclotron waves that propagate more or less along the magnetic field lines and that therefore can be detected on the ground, these recently discovered waves propagate in a direction perpendicular to the dc magnetic field and are observable only on board spacecraft. In the VLF range,

Copyright 1982 by the American Geophysical Union.

Paper number 2A0657. 0148-0227/82/002A-0657\$05.00

electrostatic waves with such characteristics have been thoroughly analyzed [i.e., Kennel et al., 1970; Fredricks and Scarf, 1973; Shaw and Gurnett, 1975; Christiansen et al., 1978; Kurth et al., 1980]. Their possible emission mechanisms have been discussed in great detail [i.e., Ashour-Abdalla and Kennel, 1978; Rönmark et al., 1978; Hubbard and Birmingham, 1978; Hubbard et al., 1979] as well as their influence on the diffusion and acceleration of electrons [Ashour-Abdalla et al., 1980].

In the ULF range the situation is quite different although waves propagating in a direction perpendicular to the dc magnetic field have a similar importance with respect to the dynamics of protons. There are few experimental observations, and the theoretical implications of the existence of these waves has been underemphasized. In the frequency range between the proton gyrofrequency and the lower hybrid frequency, electrostatic as well as electromagnetic waves can propagate in directions perpendicular to the magnetic field. The purpose of this paper is to bring new material relevant to this category of phenomenon.

The reasons for a lack of observations in this frequency range are easy to understand. There are two types of equipment able to detect the magnetic components of ULF waves in space: dc magnetometers and ac search coils. The dc magnetometers that were carried on different spacecraft have not enough sensitivity nor sufficient frequency coverage for the detection of weak magnetic fields ($< 0.5\gamma$) in this frequency range (see the introduction of Young et al. [1981]). Search coils are well suited for the detection of ac magnetic fields, in the upper part of the ULF spectrum ($f \ge 20 \text{ Hz}$), but their sensitivity decreases in the lower part of the spectrum. Besides, in the Pc 1 frequency range (a fraction of hertz) one is usually faced with the spurious and intense signal induced at the spin frequency by the rotation of the antennas in the dc magnetic field. The advantages of the GEOS search coils in this respect are (1) to have a good noise figure in the low-frequency part of the ULF spectrum $(< 10^{-2} \gamma \cdot Hz^{-1/2} \text{ at 1 Hz and} < 10^{-3} \gamma \cdot Hz^{-1/2} \text{ at 8 Hz } [S-1]$ 300 Experimenters, 1979]) (2) to be almost insensitive to the spin-induced signal, because of the existence of an onboard 'despin' system and of the implementation of efficient algorithms at the processing stage [Robert et al., 1979].

In addition to the search coil magnetometer the two GEOS spacecraft are equipped with a dc magnetometer, electric antennas, with two instruments for measuring the cold plasma density and with two sets of particle detectors to cover the energy range of interest (~ 1 to ~ 50 keV) for ions [Knott, 1975].

Among the quasi-monochromatic ULF waves which have been detected onboard GEOS 1 and 2 [Perraut et al., 1978; Gendrin et al., 1978; S-300 Experimenters, 1979] one category consists of ion cyclotron waves (ICW). They are polarized in a plane perpendicular to the dc magnetic field, usually with a left-handed circular polarization when observed at the equator and with a linearly polarized or a right-handed polarization when observed at high magnetic latitudes. Their frequency lies below the proton gyrofrequency F_{H^+} , close to the He⁺ gyrofrequency. They have been found to be associated with the presence of thermal or suprathermal He⁺ ions [Young et al., 1981]. The second category of waves, which are the subject of the present paper, have quite different characteristics. They are mainly polarized along the dc magnetic field B₀ (i.e., they propagate in directions perpendicular to B₀) and their circular component is always righthanded. They have frequencies above F_{H^+} and present a harmonic structure. They are observed only in the vicinity of the mangetic equator.

The existence of waves with similar characteristics was reported long ago, but the number of publications, dealing at least with the observational aspects of these waves, is very limited. By analyzing 29 orbits of OGO 3 during which data transmitted at high bit rate were available for the dc magnetometer, Russell et al. [1970] were able to describe some of the characteristics of a ULF noise occurring only in the vicinity of the magnetic equator (at L values between 3.8 and 5.1) with wave normal vectors almost perpendicular to \mathbf{B}_0 . A line structure was detected but only in one case a clear harmonic structure between the different components of the noise was identified (their Figure 9). Extending this study to lower L values (from 2 to 3.5) with the help of some 15 events detected onboard IMP 6 and Hawkeye 1, Gurnett [1976] was able to confirm some of these characteristics and also to present spectrograms by showing a large number of harmonics. The frequency spacing between these harmonics (extending from ~ 2 to ~ 16 Hz) was not satisfactorily identified, and no extensive study of these phenomena was ever pursued. An explanation of the origin of these waves was given in neither of these two papers. Gul'elmi et al.

[1975] were the first to propose a mechanism that accounts for the generation of these waves. The possible consequences of these waves on energetic electrons [Russell et al., 1970] or heavy ions [Gurnett, 1976] were also discussed.

Another attempt to study equatorial ULF/ELF emissions was made with the Explorer 45 search coil experiment [Taylor et al., 1975; Taylor and Lyons, 1976]. The poor sensitivity of the experiment (only waves with amplitudes larger than 0.4γ were reported) and the lack of frequency resolution (signals were integrated in two frequency bands from 1 to 3 Hz and from 3 to 10 Hz) did not allow a precise study of these emissions. However, two categories of waves were distinguished. The first was identified as ICW's, generated below the proton gyrofrequency within the plasmasphere. The second, going to higher frequencies and generated outside the plasmapause, is possibly related to the structured emissions discussed above and is the subject of the present paper.

This paper contains three main sections. In section 2, the wave characteristics are analyzed. After a brief summary of the experimental technique, some typical events are presented. The polarization and frequency structure of these emissions are described. A statistical study is done of their occurrence as a function of radial distance, magnetic latitude, and local time. Section 3 is devoted to the presentation of particle data associated with these events. The two particle experiments, one in the low-energy range ($E \leq 20$ keV) and the other in medium energy range ($E \ge 20 \text{ keV}$), are described as well as the technique used for deducing isodensity curves in the v_{\parallel} , v_{\perp} plane. The characteristics of the proton distribution functions associated with the wave events are described. In section 4 a model is presented in terms of which the observed emissions are interpreted as magnetosonic waves excited at multiples of the proton gyrofrequency by ring distributions.

2. ULF WAVE OBSERVATIONS

2.1. Experimental Technique

Both magnetic and electric fluctuations in the ULF range are continuously recorded on the GEOS satellites, up to ≈ 11.6 Hz (the sampling frequency is ≈ 23 Hz). The three magnetic components (B_Z parallel to the spin axis of the spacecraft, B_X and B_Y in the plane perpendicular to the spin axis) are measured, whereas only one electric component is detected: E_Y , perpendicular to the spin axis.

Technical characteristics for both magnetic and electric antennas are given elsewhere [S-300 Experimenters, 1979]. We only mention here that at 2 Hz the sensitivity for the magnetic components is $5 \times 10^{-6} \cdot \gamma^2/\text{Hz}$. The analyzing procedure applied to the magnetic data on a routine basis is described by Robert et al. [1979]. It mainly gives rise to grey scale plots (see Figure 1) in a frequency versus time representation; the larger the power of the signal, the darker the corresponding signal on the spectrogram. B_R and B_L are the right-hand and left-hand polarized components, respectively, of the wave in the plane perpendicular to the spin axis. These components are obtained by combining the measured signals B_X and B_Y according to a technique that was defined by Kodera et al. [1977]. The proton gyrofrequency (as deduced from the dc magnetometer experiment S-331) is superimposed on the spectrograms. The value of the power spectral density (psd) that corresponds to the darker level (black) is indicated in the caption. It corresponds to the 0-dB

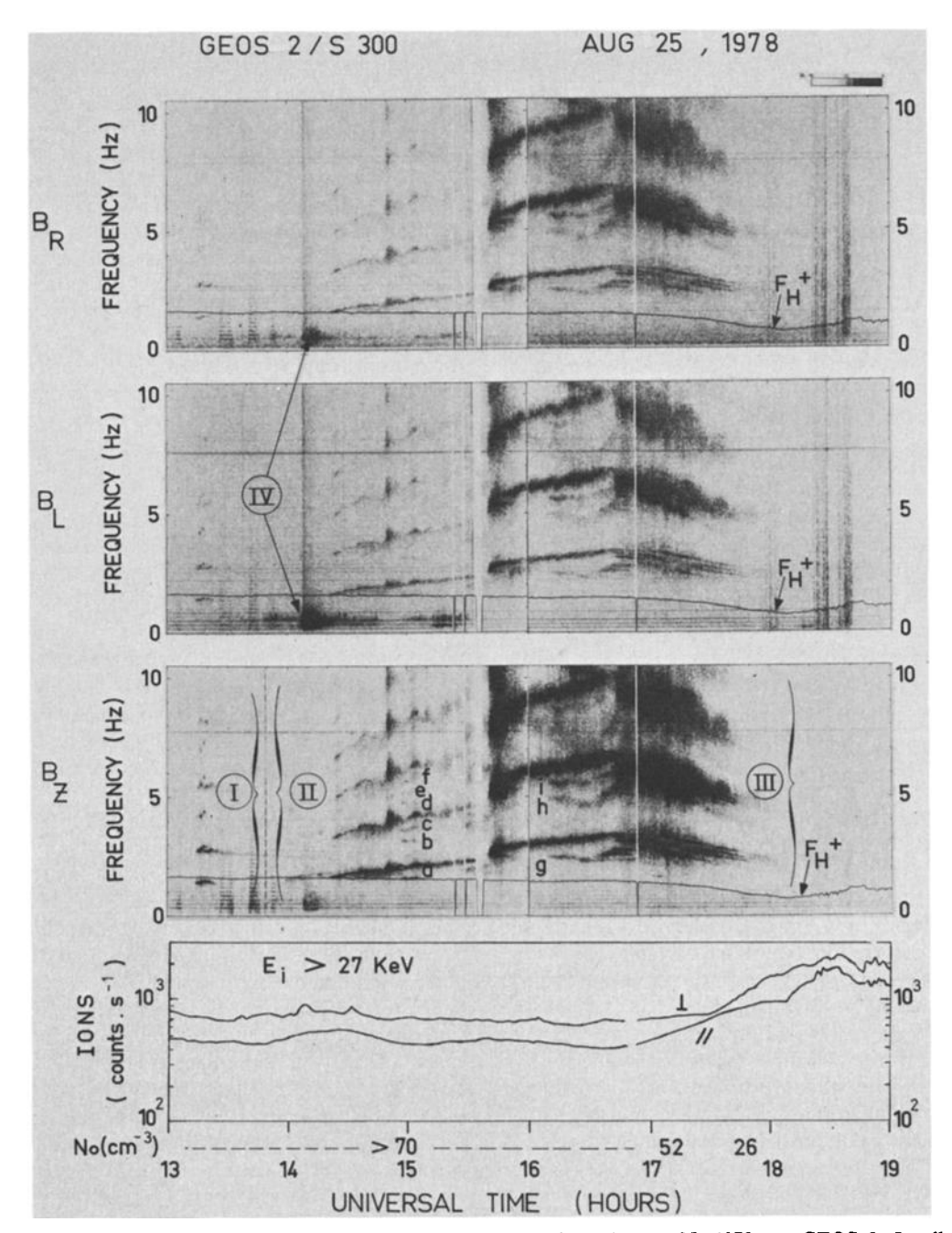


Fig. 1. Frequency-time spectrograms of ULF waves observed on August 25, 1978, on GEOS 2. In all such spectrograms the frequency range is 0 to 10.5 Hz. Intensity reference level (black) is $10 \gamma^2/\text{Hz}$ at 1 Hz. The three panels refer either to the circular components that are right handed (B_R) , left-handed (B_L) in the plane perpendicular to the spin axis, or to the component that is parallel to the spin axis (B_Z) . The angle between the spin axis and the dc magnetic field θ is $\sim 13^\circ$, the distance $6.6 R_E$, and the magnetic latitude $\lambda m = -3^\circ$; LT = UT + 2 hours, 25 min. Integral proton fluxes perpendicular and parallel to B_0 are also plotted. The cold plasma density N_0 is high during the event. Harmonic emissions I, II, and III are strongly polarized along B_Z , i.e., along the dc magnetic field, and are considered as magnetosonic waves. Event IV is left handed and is identified as ICW's (The faint line at ≈ 7.8 Hz is a spurious signal).

level of the grey scaling grid, which is presented on the top of the figures, and it is usually different for the three components. Note that this number is valid for an emission at 1 Hz and that in order to obtain the correspondence between the same grey level at another frequency and the psd, one must multiply it by $1/f^2$. This is due to the fact that the higher frequencies have been artificially enhanced, on these grey-scaling plots, in order to balance the tendency of natural emissions to be less intense at higher frequencies.

The angle θ between the spin axis and the static magnetic

field is usually very small on GEOS 2, but it can be large (30°) on GEOS 1. Thus, in order to identify without ambiguity the polarization of the signal, it is sometimes necessary to perform a change of reference frame. This has not been done on a routine basis, but the spectra of selected events have been displayed in a reference frame where B_Z is aligned with the dc magnetic field.

As the spacecraft longitude has been changed a few times, the relation between LT and UT may differ for different events.

2.2. Description of Typical Events

In this paragraph, some events are presented in order to illustrate the general characteristics of magnetosonic ULF emissions.

2.2.1. August 25, 1978 (Figure 1): LT = UT + 2.25. This case illustrates the complexity of these kinds of emissions. It occurred during a weak storm starting around 09.00 UT (Kp = 30 between 12.00 and 15.00, Kp = 2+ between 15.00 and 18.00). A strong ring current injection occurred between ~17.00 and 19.00 as evidenced by the increase of the flux of protons (E > 24 keV) and by the decrease of F_{H^+} , the dc magnetic field B_0 changing from 105 γ at 17.00 to 50 γ at 18.00. The wave event itself can be divided into four independent emissions.

Emission I consists of very monochromatic, harmonically related emissions starting at 1315 UT. The spectrograms show that the B_Z component is stronger than the B_L and B_R components. This is more clearly evidenced on an amplitude versus frequency plot taken around 1318 UT, in which a frame of reference with the Z axis parallel to B_0 has been used (Figure 2). The parallel component is 20 to 30 dB larger than B_R which in turn is 6 to 10 dB larger than B_L . The amplitude of the harmonics decreases with the order of the harmonic at a given time, the odd harmonics disappearing first as time elapses (throughout this paper we will define the nth harmonic as the one whose frequency is equal to n times the fundamental).

Emission II starts around 14.15, with a fundamental frequency equal to the local $F_{\rm H^+}$. Its frequency increases with time and then decreases (apparently it is the same event which continues until ~1700 UT). Again the B_Z component is larger than B_R or B_L (at 1450 UT f.i. $B_Z = 95$ m γ , $B_R = 18$ m γ , $B_L = 3$ m γ for the fundamental). The second harmonic has still a large amplitude ($B_Z = 50$ m γ at 1450 UT).

Emission III starts at 1540 UT, just after a telemetry drop out. At that time $B_Z=350~{\rm m}\gamma$, $B_R=38~{\rm m}\gamma$ for the fundamental, and $B_Z=170~{\rm m}\gamma$ for the second harmonic. This emission is strong, and their spectra are rather broad. The frequency increases with time until $\sim 1645~{\rm UT}$ (a time at which the fundamental approaches $2~F_{\rm H^+}$), whereas the local proton gyrofrequency remains constant. A fine structure is visible in the last part of the emission, as it was the case for

emission II near 1500 UT. These structures, which seem to be produced by a wave-wave coupling mechanism, will be discussed later.

The fourth emission is of a completely different nature. Its frequency is much smaller than F_{H^+} . It has no harmonic structure, and it is mainly polarized in the plane perpendicular to B_0 , with a tendency for the left-handed polarization to be stronger than the right-handed one.

This illustrates the fact that there are two kinds of quasimonochromatic emissions in the ULF range: the ion cyclotron waves (emission IV), which are extensively described by Young et al. [1981], and the waves that are the subject of the present paper (emissions I, II, III). Another example of an almost simultaneous occurrence of the two types of waves with their different polarizations is given elsewhere [Gendrin, 1980, Figure 3]. Because the B_Z component is the strongest one for these waves, it is the only one that will be displayed for the following examples.

2.2.2. August 9, 1978 (Figure 3a): LT = UT + 1.11. The emission occurs above 3 Hz with a frequency separation Δf between the different bands close to the proton gyrofrequency F_{H^+} . These bands seem to be harmonically related to a fundamental at $f_0 = \Delta f \approx F_{H^+}$, which is not detected. This fact demonstrates that the observed harmonic structure is real; i.e., it is not due to a saturation effect in the electronics or in the analyzing procedure. The wave has a weak intensity. The strongest bands have a B_z component equal to 30 m γ (at 4.3 Hz and 2249 UT) and to 12 m γ (at 7.8 Hz and 2400 UT). The cold plasma density measured by the S-301 experiment is very low ($\sim 2 \text{ cm}^{-3}$).

One may also notice that this emission contains short duration elements with a dispersive structure.

2.2.3. August 20, 1978 (Figure 3b): LT = UT + 2.04. This event is interesting because it also shows that all the harmonics are not always present and that during the course of the event some other harmonics may appear. At 1850 UT there are only two lines, labelled a and b, which are harmonically related. Some 13 min later, lines c, d, e, and f appear. Clearly, all these lines are harmonically related. For instance, at 1925 UT, their frequencies are multiples of the same frequency $f_0 = 1.16$ Hz; this is slightly lower than the local proton gyrofrequency (1.36 Hz). It is interesting to note that the strongest lines near 1900 UT (lines a and b) and near

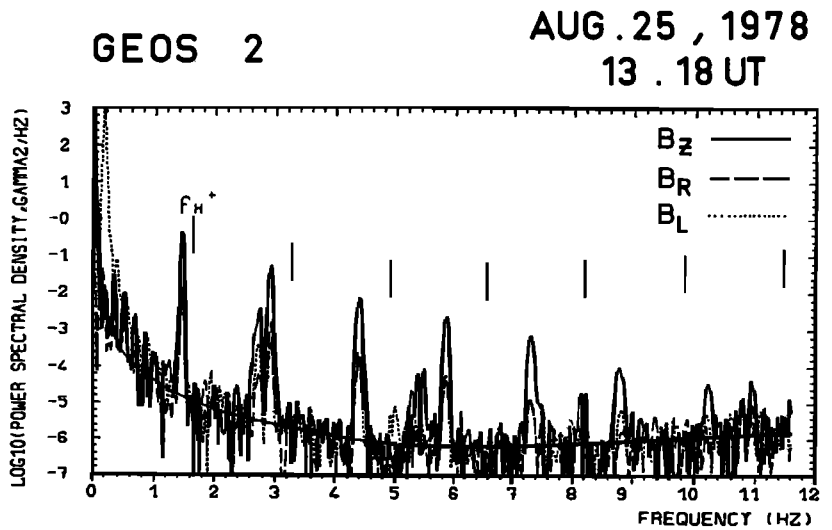


Fig. 2. Power spectrum for a 44-s time interval selected from data of Figure 1. A change of the reference frame was performed, leading to a B_Z component aligned with the dc magnetic field (see text).

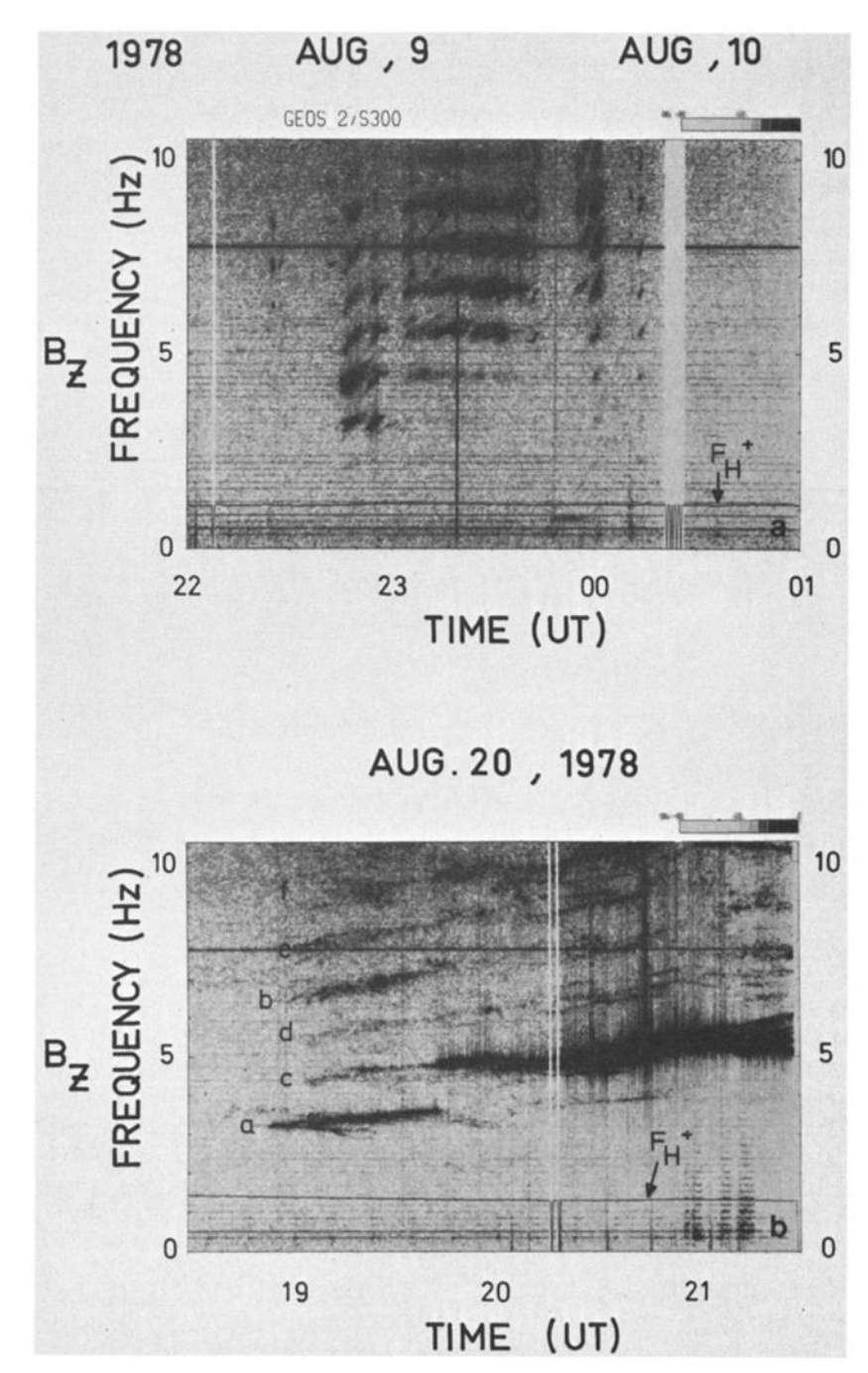


Fig. 3. Frequency-time spectrograms of the B_Z component for two different events. (a) August 9, 1978, emissions occur at $\lambda m = 0^\circ$, at $6.6 \, R_E$ and $\theta \simeq 13.5^\circ$; LT = UT + 1 hour, 11 min and $N_0 \simeq 2 \, \mathrm{cm}^{-3}$. The black reference level is 0.05 γ^2 /Hz at 1 Hz. This kind of successive short duration events is typically observed in the night sector. One may note the absence of fundamental and first harmonics, which is evidence that these structures are not generated by nonlinear effects within the electronics. (b) August 20, 1978, event occurs at $\lambda m = -2^\circ$, $\theta \simeq 11^\circ$. TL = UT + 2 hours, 04 min and $N_0 \simeq 8 \, \mathrm{cm}^{-3}$. The black reference level is 0.1 γ^2 /Hz and 1 Hz. At 1900 UT, emissions a and b and at 2000 UT emissions c and f are harmonically related.

2000 UT (lines c and f) are themselves harmonically related.

The amplitude of the most intense wave is continuously increasing from $\sim 20~\text{m}\gamma$ at 1900 UT to 90 m γ at 2045 UT. The cold plasma density is rather high ($\sim 8~\text{cm}^{-3}$) and stable for such a night time event ($\sim 2100 < \text{LT} < 0100$).

2.3. General Characteristics

Here we will report characteristics of the harmonic emissions that are deduced from the examination of hundreds of events.

2.3.1. Polarization. As clearly evidenced on Figures 1 and 2, the magnetic component of the kind of emission which is studied in this paper is almost aligned with the dc magnetic field \mathbf{B}_0 , contrary to ICW's whose magnetic component is contained in the plane perpendicular to \mathbf{B}_0 . The wave vectors of these emissions are therefore orthogonal to \mathbf{B}_0 . The B_R component of these waves is generally weak, but it is still larger than the B_L component, which indicates that the waves are right-hand polarized.

The amplitude of the electric component of these waves is

usually below the sensitivity threshold of the electric field experiment (2 × 10⁻⁴ V m⁻¹ Hz^{-1/2} around 1 Hz). For instance, if one assumes that the phase velocity of the wave v_{ϕ} is ~ 1000 km s⁻¹, the electric sensor will respond only to waves whose magnetic component is larger than 2 × 10⁻⁴/ 10^6 T Hz^{-1/2} $\approx 0.2 \gamma$ Hz^{-1/2}. Typical spectral power densities are usually smaller than this value. Consequently, these waves are not, in general, detected by the electric field experiment. However, strong events can be also detected by the electric antennas; in this case, the ratio E/B has been found to be close to the Alfven velocity V_A (D. Jones, private communication, 1980).

All these characteristics are those expected for waves propagating in the magnetosonic mode. Henceforth these emissions will be designated as magnetosonic waves (MSW).

2.3.2. Harmonic structure. The harmonic structure of MSW's detected on board GEOS is a general feature, which can clearly be identified on the spectrograms. The three events 1, 2, and 3 of Figure 1 are good examples of such a behavior, which does not depend on the frequency of the fundamental. The first event is just below F_{H^+} ; the second event, which also starts below F_{H^+} , has a frequency that increases with time and that crosses F_{H^+} . The fundamental of the third event is well above the local proton gyrofrequency.

Obviously, it has been checked that these harmonic structures are not due to nonlinear effects occurring in the detecting system. Indeed, for most of the events, the signals are not very intense, the amplifier is in its highest gain configuration.

On Figure 4, the spectrum of another typical event is plotted. The spectral power density has its maximum not at the frequency of the fundamental but at the 3rd and 4th harmonics. We have seen that frequencies corresponding to the fundamental may not be even visible. This is another proof that the harmonic structure is real and that it is not produced by the electronics.

As will be shown later the number of harmonics can be large (>8) so that the spectrum may extend well above the Nyquist frequency f_{NY} (= 11.6 Hz) of the ULF experiment. Consequently, aliasing effects can occur: a strong signal at a

frequency $f > f_{\rm NY}$ will induce an apparent signal at the frequency $2f_{\rm NY}-f$. Indeed such effects have already been observed [see *Perraut et al.*, 1978, Figure 8]. Another example is shown Figure 5. The waves above 5 Hz, which are polarized along ${\bf B}_0$, consist of quasi-monochromatic emissions that exhibit a complex frequency-time structure with both increasing and decreasing frequencies. The strongest decreasing signal (a) around 8 Hz is observed at its real frequency: $F = 4 F_{\rm H^+}$. Conversely, signals with increasing frequencies (b, c, and d) are due to the aliasing effects; for instance the lowest frequency ($F \sim 6$ Hz) can be understood as an image at frequency $F \approx 2 F_{\rm NY} - 9 F_{\rm H^+}$ of a signal at a frequency $F \approx 2 F_{\rm NY} - 9 F_{\rm H^+}$ of a signal at a frequency 9 $F_{\rm H^+}$ and similarly for the other two which are images of the 8th and 7th harmonics.

2.3.3. Frequency range. The waves that we are studying have their fundamental around or above F_{H^+} . Occasionally, these emissions can be detected well below F_{H^+} , with a fundamental between F_{He^+} and $2\,F_{He^+}$, in a frequency range where ICW's are generally observed. Conversely, ICW's that are left-handed polarized in the plane perpendicular to \mathbf{B}_0 can be sometimes detected just below F_{H^+} . This is clearly illustrated in Figure 5. Thus the frequency domain of the two kinds of waves overlap. However, and despite some exceptions, one can say that MSW's occur above F_{H^+} , whereas ICW's are observed well below F_{H^+} . But is it better to characterize MSW's by their polarization than by their frequency.

As said above, the frequency range covered by the emission can well exceed the frequency range of the ULF experiment. But there is another amplifier, onboard GEOS, that is operated from time to time and that gives the wave form of the signals in the frequency range from a few hertz to 450 Hz [Cornilleau-Wehrlin, 1981]. On some occasions this amplifier did operate at a time during which MSW's were detected by the ULF experiment. The corresponding spectrum, integrated over 20 s, is presented on Figure 6. In this event, three harmonically related emissions occur simultaneously, the fundamentals being at frequencies $f_1 = 9.45$ Hz, $f_2 = 11.65$ Hz, and $f_3 = 13.25$ Hz. Harmonics up to $5 f_1$, $4 f_2$, and $3 f_3$ are visible. This shows that even at the geostationary orbit, harmonically related emissions can have

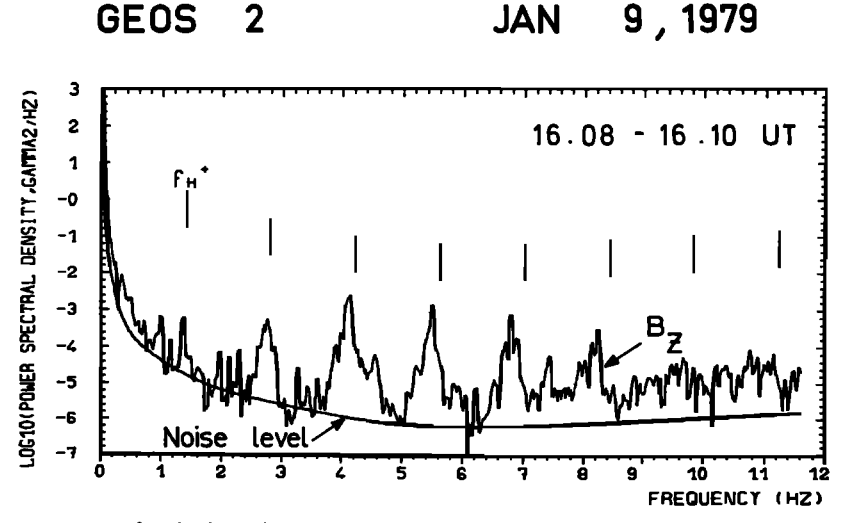


Fig. 4. Power spectrum for the interal 1608-1610 UT on January 9, 1979 (spectrogram not shown). At this time GEOS 2 was located at $\lambda m \simeq -2^{\circ}$ and LT = UT + 2 hours, 26 min. A change of reference frame was performed to align the B_Z component with respect to B_0 .

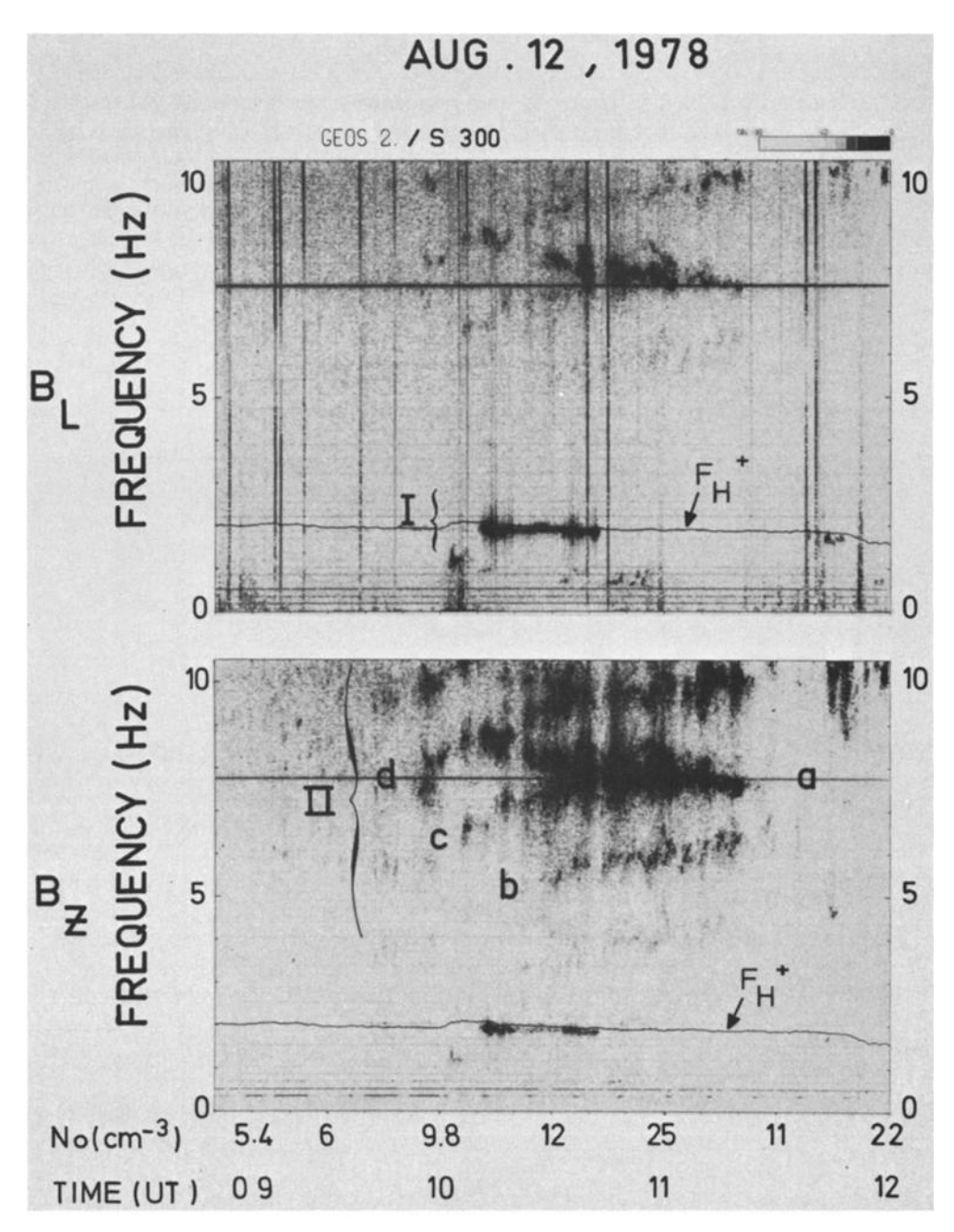


Fig. 5. Frequency-time spectrograms of the B_L and B_Z components for August 12, 1978, on GEOS 2. The black reference level is 0.3 γ^2/Hz at 1 Hz. $\theta \simeq 12^\circ$, $\lambda m \simeq 0^\circ$, and LT = UT + 1 hour, 22 min. Two different events are detected simultaneously. Although close to F_{H^+} , the event I is clearly left-handed polarized in the plane perpendicular to B_0 and therefore belongs to ICW. At larger frequencies a NSW is observed that is polarized along the static magnetic field. In spite of the complexity of the event II, an harmonic structure can be recognized (see text).

frequency components up to 50 Hz at least, confirming the original discovery of Russell et al. [1970] at L values around 5.

2.3.4. Nonlinear coupling. When the signals are strong, an harmonic structure may be the consequence of wave-wave coupling; this is particularly true when the waves are monochromatic because the coupling process is then coherent. Figure 6 illustrates this effect. If one calls $f_i(j = 1)$, 2, 3) the frequencies of the fundamentals, one observes emissions at the frequencies $f_j + f_k$ and $3 f_j + f_k$. The spectrogram of Figure 7 shows another example

observed on August 23, 1978. The emission starts at 1537

UT, exactly at the proton gyrofrequency. From thereon it splits up into three independent emissions. The first has a frequency which decreases with time; let us call it the emission at f_1 . The two others have a frequency which increases with time, f_2 and f_3 . As time proceeds a number of other lines appear. A strong intensity enhancement occurs when the line 2 f_1 merges with the line f_3 . A detailed spectrum, (Figure 8) taken around 1637 UT and integrated over 44 s shows that (1) harmonics up to 9 f_1 , 6 f_2 and 5 f_3 are visible, and (2) almost all the combinations $nf_j + f_k$, where n = 2, 3, 4, are observed.

Although the signals are rather strong (the fundamental

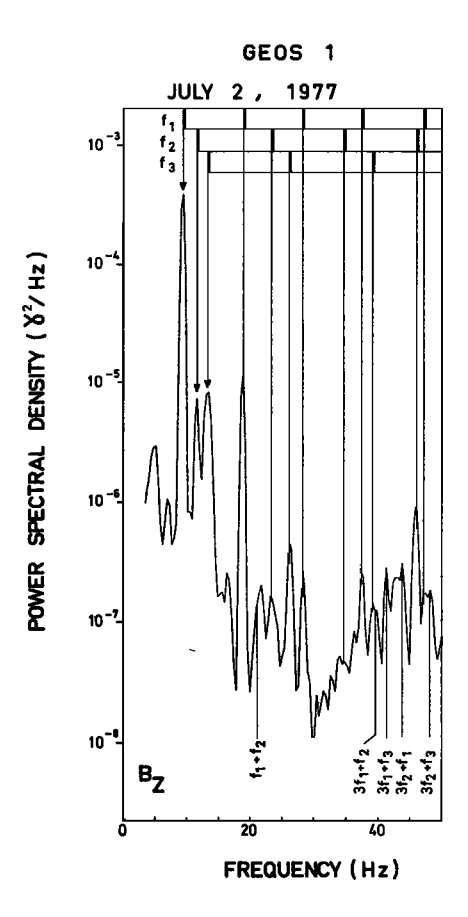


Fig. 6. Power spectrum (up to 50 Hz) integrated over 20 s for the July 2, 1977, event around 1100 UT; $\lambda m \simeq -6^{\circ}$, LT = 1348. Three fundamental frequencies f_1 , f_2 , and f_3 and their harmonics can be distinguished. Different couplings between these three emissions are also observed.

at f_0 reaches 0.5 γ Hz^{-1/2}) they are still some 30 dB below the saturation of the amplifier and telemetry systems, so that this nonlinear coupling is not of experimental origin.

Let us summarize the properties of these observed ULF waves: their magnetic field is almost aligned along the static magnetic field B_0 and the weak component in the plane perpendicular is right-hand polarized. They are harmonically related and the fundamental is generally around or above the proton gyrofrequency. The fundamental and lower harmonics may sometimes be missing. When several emissions are simultaneously present, with different fundamental frequencies, wave-wave coupling may occur.

2.4. Statistical Study

This study is made with the help of both GEOS spacecraft. GEOS 2 being at an almost constant and low magnetic latitude will help us to find the local time dependence of these events. On the contrary, GEOS 1, which explored a wide range of magnetic latitudes (λ_m) and radial distances (R), will be used to study the R, λ_m dependence of the harmonic emissions.

2.4.1. Dependence on radial distance and geomagnetic latitude. The GEOS 1 satellite has explored regions between $L \sim 4$ and $L \sim 8$, in a magnetic latitude range $-15^{\circ} < \lambda_m < +30^{\circ}$. We therefore had the opportunity to investigate if these harmonic emissions could be detected, within the explored volume. On Figure 9, the range of geomagnetic latitude and geomagnetic local time that was explored by GEOS 1 between May and October 1977 is represented. The hatched areas correspond to regions that were inaccessible because GEOS 1 was not visible from the Darmstadt receiving station. Note that in fact in the regions corresponding to $L \leq 4.5$, we do not have any valid measurement, because the spacecraft was entering the inner magnetosphere for which

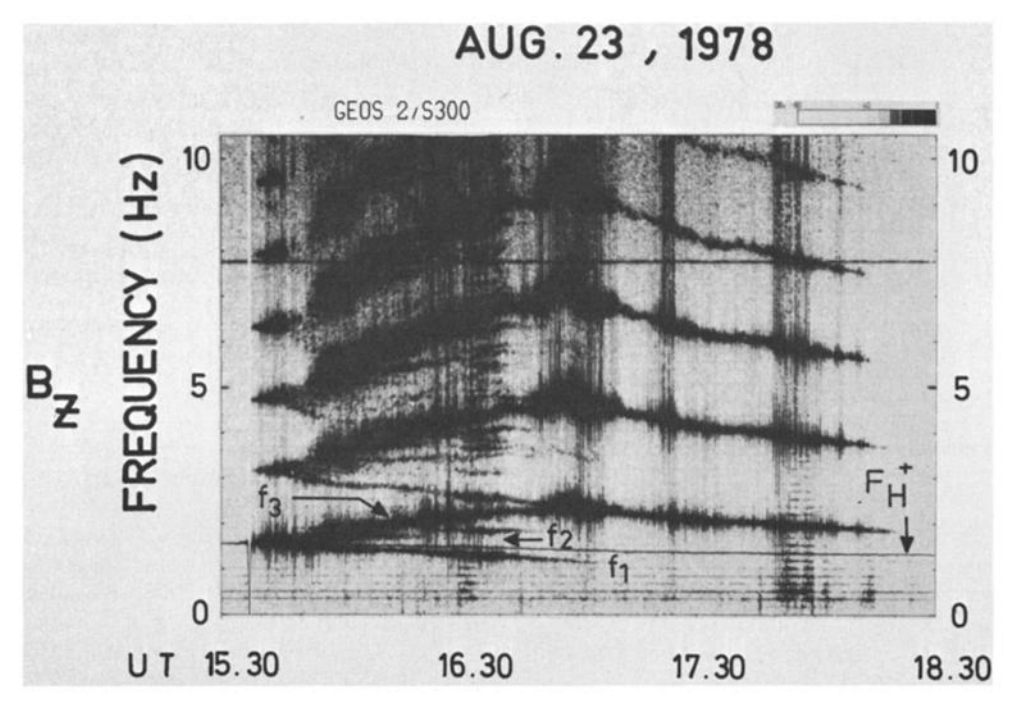


Fig. 7. Frequency time spectrogram for August 23, 1978. The black reference level is 0.1 γ^2/Hz at 1 Hz; $\theta \approx 12^\circ$, $\lambda m \approx -3^\circ$, LT = UT + 2 hours, 18 min, and $N_0 \approx 45 \text{ cm}^{-3}$. Three different fundamentals f_1 , f_2 , and f_3 can be distinguished, leading harmonic production and wave-wave coupling to many lines, especially around 1630 UT.

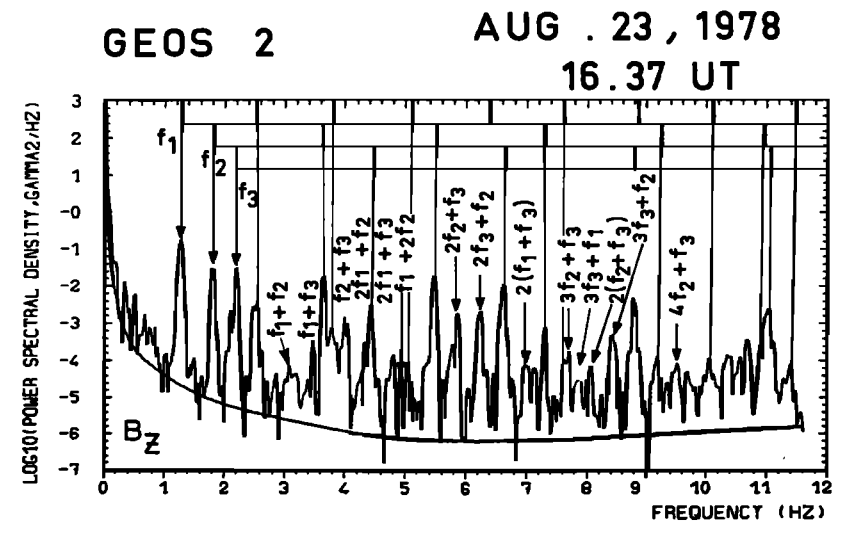


Fig. 8. Power spectrum for a 44-s time interval selected within the event presented on Figure 7, at 1637 UT. A change of reference frame was performed to align B_Z with respect to B_0 .

its equipments were not expected to function. The boundary curves between accessible and inaccessible regions have a smooth seasonal variation. However, they do present discontinuities for the periods at which the spacecraft apogee was moved in longitude. The solid lines correspond to countours of constant geomagnetic latitude, the dashed lines correspond to countours of constant L value, and the vertical bars show the time during which strong harmonic emissions were observed. It is clear that most emissions occur in a restricted range of λ_m , i.e., when the spacecraft is in the vicinity of the magnetic equator ($|\lambda_m| < 10^\circ$). On the contrary, there does not seem to be a specific range of L values (between 4.5 and 7 at least) where these emissions can be observed, provided the satellite is not too far from the magnetic equator. These findings agree with those of Russell et al. [1970].

They have also to be compared with those of Gough et

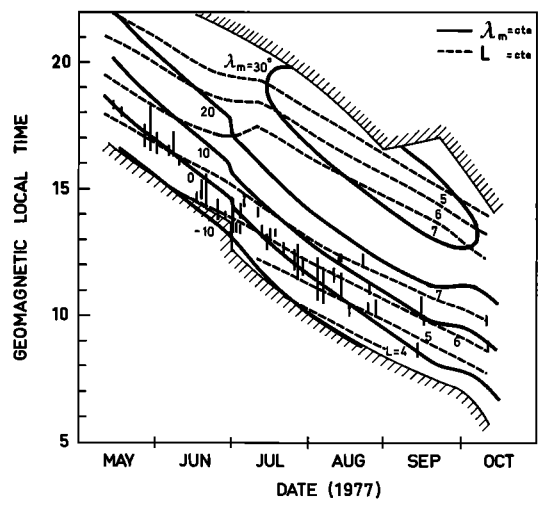


Fig. 9. Latitudinal dependence of MSWs. The geomagnetic local time intervals between the hatched area were explored by GEOS 1. The continuous lines correspond to iso-magnetic latitudes, whereas the dotted lines correspond to the iso-L values. Abrupt changes in July and September are due to a change of the longitude of the GEOS 1 apogee. MSWs are represented by vertical bars. The emissions are mainly located in the vicinity of the magnetic equator.

al.'s [1979], who studied the occurrence of VLF electrostatic emissions between the electron gyroharmonics and who also found that these emissions were concentrated near the geomagnetic equator (their figure 2).

2.4.2. Local time distribution. The study covers four months of data (August-November 1978) obtained with GEOS 2. The total number of magnetosonic waves detected in a given local time hour is represented on Figure 10a. When an event extended from one hour sector to the next one, it was counted in both sectors. The histogram shows that these events are rather common at the geostationary orbit. On the average, there is a 12% probability to detect such an event within a given hour. Magnetosonic emissions are very common and are restricted to a limited range of magnetic latitudes. They have not been measured before because of their rather low amplitude ($\leq 0.3\gamma$). The histo-

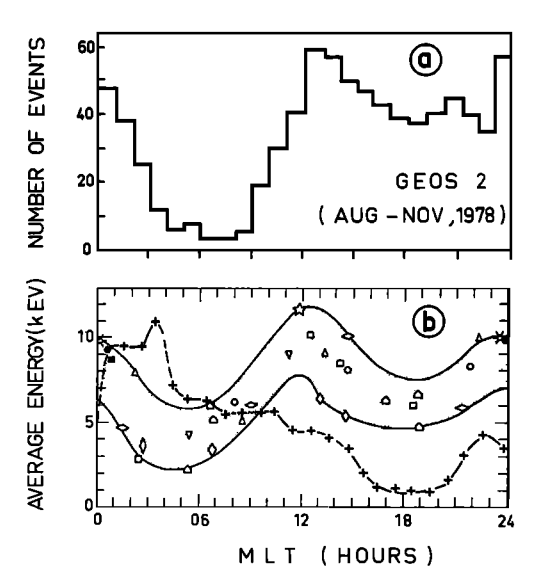


Fig. 10. Local time distribution of MSW's and their relationship with medium energy protons. The number of MSW's detected during 4 months on GEOS 2 during a given hourly interval is plotted on (a). The average energy of precipitating auroral protons (0.4 < E < 30 keV) measured on AUREOLE 1 satellite is the grey area on (b). An estimation of the Alfven energy E_A at the geostationary orbit is superimposed (cross-dashed line; see text).

gram shows that there are only a few events detected between 0300 and 0900 LT. Maxima of occurrence are observed around noon and midnight. For these periods there is a 50% probability of observing magnetosonic waves. In the afternoon and evening sectors, the probability is of the order of 30%.

In the following section we will see that the generation of these waves is directly related to the shape of the proton distribution function in the equatorial plane. Prior to illustrating this link, let us point out that there is striking agreement between the local time distribution of the waves and the variations of the mean energy of auroral protons (0.4) < E < 25 keV) as a function of the local time (Figure 10b). These last measurements were obtained at auroral latitudes by Galperin et al. [1976], on board the polar orbiting satellite AUREOLE 1 at ionospheric altitudes; nevertheless, the authors have shown that at least the most energetic component of the proton spectrum at this low altitude is similar to the spectrum that exists in the equatorial plane. Moreover, the evolution of the shape of the spectrum and of the mean energy as a function of the local time is well explained by models involving proton injection and subsequent drift from a source region in the nightside of the magnetosphere [Mauk and McIlwain, 1974]. The spectra observed in the source region and in the nightside of the auroral oval are characterized by one or several marked peaks having energies around 10 keV. These maxima are still more pronouned in the noon sector, owing to compression of the magnetic field on the dayside. In fact, the mean energy deduced from these measurements is almost equal to the energy corresponding to this maximum. However, low-energy protons, drifting eastward under corotation can directly reach the morning sector. In this local time region, for latitudes corresponding to the geostationary orbit, the observed spectra have no maximum and the average energy is rather low [Sauvaud et al., 1981].

In order to establish more quantitatively the relation between the histogram of magnetosonic waves and the local time distribution of these energy peaks for protons, it is necessary to anticipate the main result of the theoretical discussion which will be given in section 4. Magnetosonic waves can be amplified by proton distributions that present a peak at a certain energy, provided that this energy exceeds a threshold given by 1/2 m V_A^2 , the Alfven energy. This last parameter has been determined by using an averaged local time distribution of the cold plasma density with a bulge around 1800 LT, deduced from measurements obtained with the GEOS 2 relaxation sounder [Higel and Lei, 1982]. For the evaluation of the magnetic field we have used the regular daily variation observed at the geostationary orbit. In these conditions, the Alfven energy presents (cross-dashed lines on Figure 10b) a well pronounced minimum around 1800 LT and remains below the proton average energy curve between 0900 and 2400 LT, therefore magnetosonic waves can be amplified in this region of the magnetosphere. In the morning sector the Alfven energy is above the mean energy of protons, thus the waves cannot be generated.

3. Energy Source of Magnetosonic Waves

3.1. Proton Data Presentation

The wave phenomena described above occurred near the proton gyrofrequency and its harmonics. Therefore protons in the keV energy range are likely to destabilize them.

Furthermore, since their phase velocity is close to the Alfven velocity the energy of these protons must exceed the Alfven energy (see Figure 10b). In order to identify the energy source of these magnetosonic emissions we have undertaken a careful analysis of the shape of the proton distribution function.

The two-dimensional particle data analyzed in this section were measured on board GEOS by the following two experiments: (1) S-310 (Kiruna Geophysical Institute), which covers the proton energy range from 0.3 to 20 keV, and (2) S-321 (Max Planck Institut für Aeronomie), which covers the proton energy range from 20 to 3300 keV.

The S-310 experiment has been described in detail by Borg et al. [1978, 1979], and only its principal characteristics will be recalled here. The spectrometers consist of a series of 10 electrostatic analyzers and associated channeltrons, pointing in different directions, with a band pass $\Delta E/E$ that varies between 9% and 27% (depending upon the analyzer), and an acceptance angle that is approximately equal to $6 \times 6^{\circ}$.

The full range of pitch angles swept during a spin period $(\sim 6 \text{ s})$ depends on the angle between the magnetic field line of force and the satellite spin axis that points to the north during the first period of the GEOS 1 mission. A good pitch angle coverage is generally obtained over one hemisphere (90–180°). The normal mode gives a full spectrum every 3 min: 32 energy levels are successively scanned, each energy level being sampled every 86 ms during a full spin period. When the characteristic time for temporal fluctuations is less than 3 min, fewer energy steps are scanned (fast mode) in order to obtain meaningful data in a shorter time interval. The energy spectra shown in this work correspond to sweeps over 8 energy levels, that is during approximately 45 s. Since several different detectors are used to obtain a wide pitch angle coverage, all the data have been corrected. In a first step, a correction has been applied in order to avoid the contamination due to solar UV and high-energy cosmic rays. Then each individual count relative to a given detector is intercalibrated with respect to those of D2-D8 group, with D-7 as a reference. Finally a full energy-angle matrix is obtained: 32 (or 8) energy levels for each of the 18 pitch angle

A second charged particle spectrometer detects energetic protons (> 20 keV). It has been described by Korth et al. [1978]. This instrument contains four solid state detector telescopes with look directions relative to the spin axis of 23°, 46°, 83°, and 106°, respectively, and angular resolutions of \pm 5° in elevation and \pm 2° in azimuth. The energy distribution of the protons was determined in 11 approximately logarithmically spaced energy channels in the range from 20 keV to 3.3 MeV. For each direction the sampling time amounts to 0.344 s per 5.5 s. In addition, protons with energies > 27 keV were recorded continuously in four directions with a time resolution of 0.172 s. No identification of the different ion species was possible. For the interpretation of the data we assume that most of the ions are protons. This assumption is supported by a direct comparison of fluxes with the mass spectrometer (a complete discussion is found in section 4b of Balsiger et al. [1980]). While we cannot rule out the presence of heavy ions, based on the above arguments they probably contribute less than 10% to the energetic ion fluxes reported here.

From the differential energetic spectra obtained over 45 s or 3 min for S-310 or over some 5 min for S-321, the phase

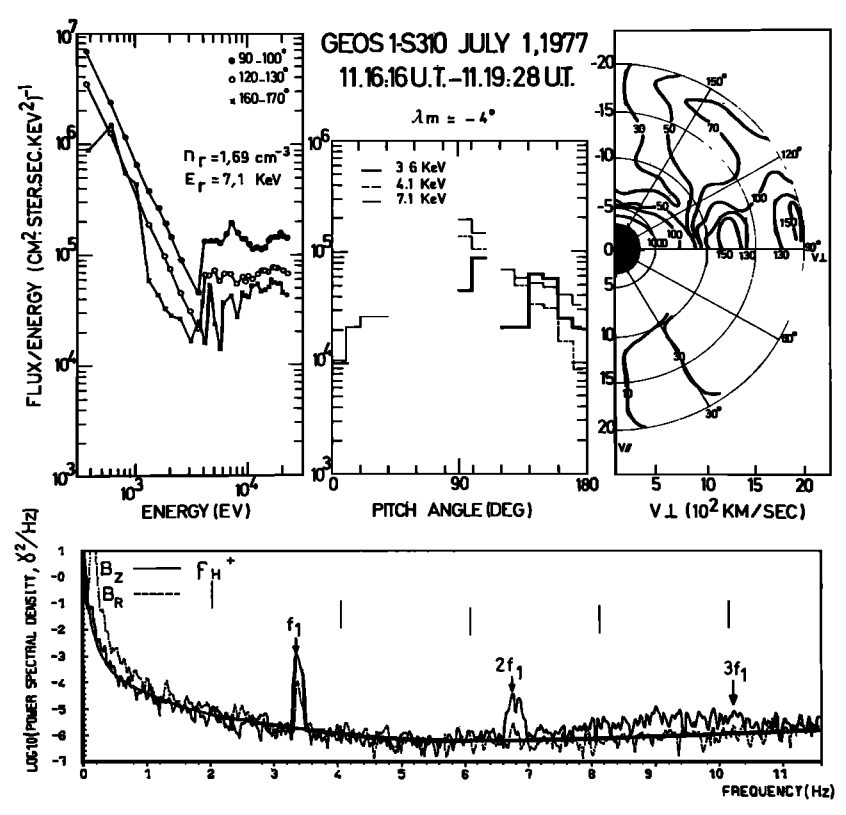


Fig. 11. Comparison between MSWs and energetic protons July 1, 1971. The energy, pitch angle distributions, and distribution functions f(V) in the velocity space measured over ~ 3 min are drawn on the top. Two-dimensional isocontours of $f(v_{||}, v_{\perp})$ are labelled in units of 10^3 (cm² s sr keV²)⁻¹. A peak at 7 keV and on the 90° pitch angle is clearly seen (two left panels). Two different maxima in the direction perpendicular to \mathbf{B}_0 are evidenced (right panel). $\partial f/\partial V_{\perp}$ is > 0 in the close vicinity of these peaks. The wave power spectrum computed simultaneously is drawn below. A change of reference frame was performed to align B_Z with respect to $\mathbf{B}_0 \cdot F_{H^+}$, and its harmonics are also plotted.

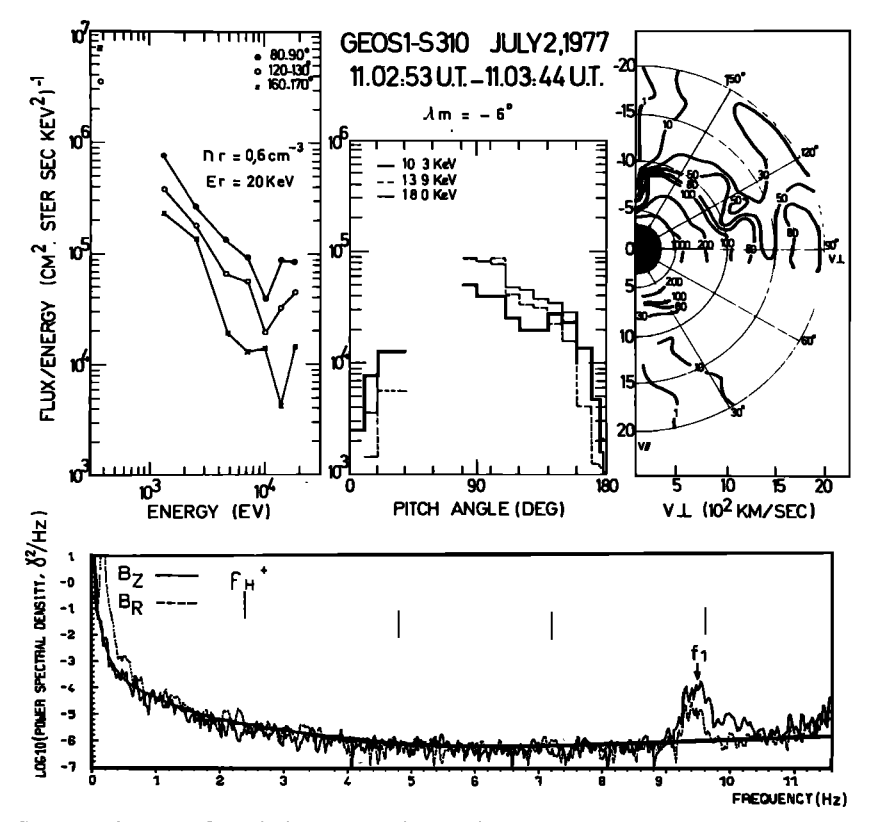


Fig. 12a. Same as Figure 11, for July 2, 1977. Again a peak at 18 keV is observed on the three kinds of plots. The wave power spectrum until 11.6 Hz is plotted in the frame aligned with respect to B_0 . The power spectrum above 11.6 Hz is given in Figure 6.

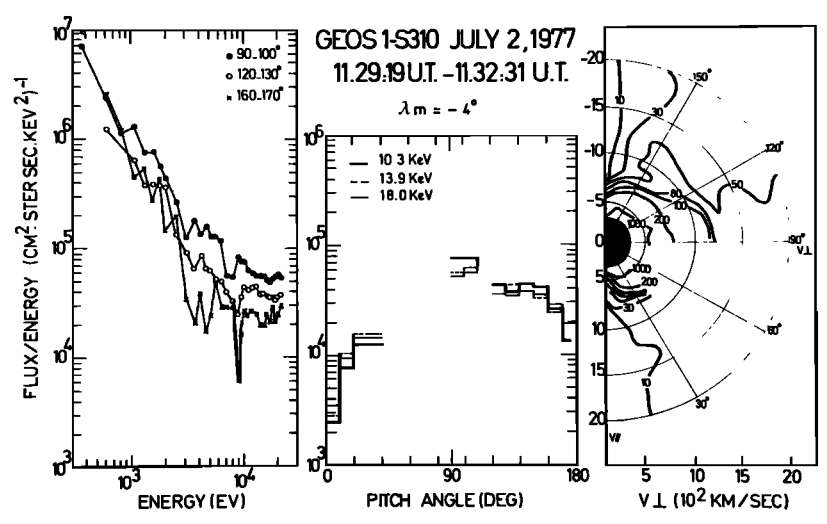


Fig. 12b. Same as Figure 11 for July 2, 1977, 27-min later with respect to Figure 12a. The particle date have a monotonic spectrum, and no waves are detected during this time interval.

space density, f(v), has easily been determined according to the relation:

$$f(v) \propto \frac{J(E, \alpha)}{E} \text{ (cm}^{-2} \text{ s}^{-1} \text{ sr}^{-1} \text{ keV}^{-2})$$

where $J(E, \alpha)$ is the flux corresponding to the central energy of the explored energy step and where one assumes that all ions are protons. Consequently, the proton data presented here consist of three complementary plots (Figures 11, 12, and 13). On the left, are represented the energy spectra for some characteristic pitch-angles: around 90° or 120° and

160°. In the middle panel the pitch angle distributions for typical energies are plotted. (In this study, the selected energies are those close to the peak of the energy spectrum, which clearly provides the free energy source). On the right, isocontours of the phase space density in the $(v_{\parallel}, v_{\perp})$ velocity space are drawn. As mentioned above, the cycle being limited to 1- or 3-min time intervals, only a portion of the $(v_{\parallel}, v_{\perp})$ space is explored during a spin period of GEOS 1 (especially between 80° and 176° during this period). This last kind of plot is of particular interest for studying waveparticle interactions, especially since $\partial f/\partial v_{\perp} > 0$, while

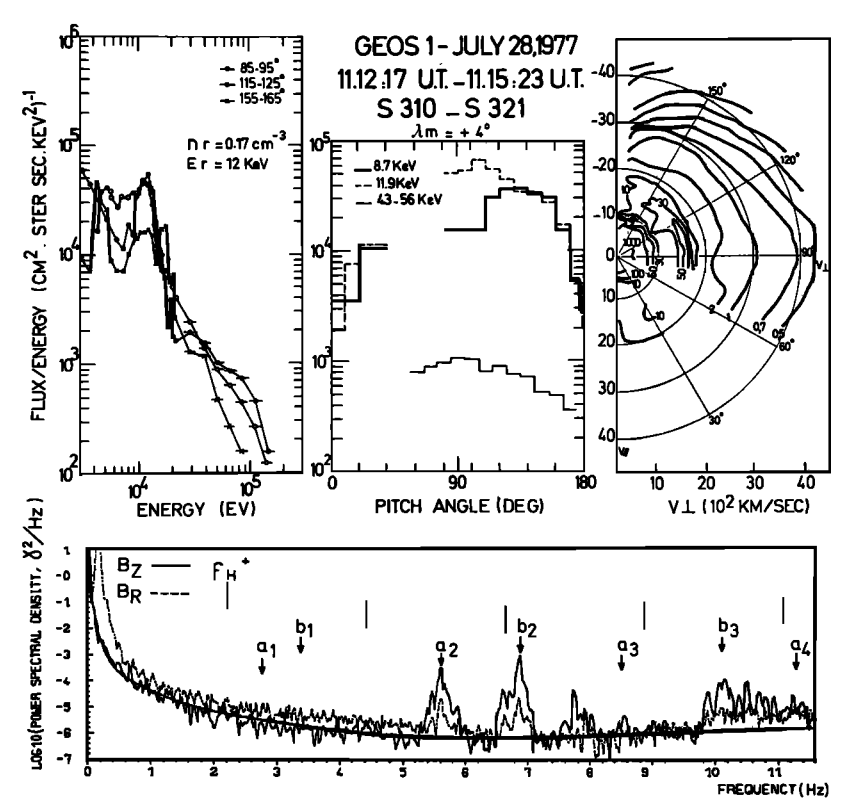


Fig. 13. Same as Figure 11 for July 28, 1977. Again a large peak at ~ 12 keV on the 90° pitch angle is observed on the three plots. The wave power spectrum drawn below is complex. It can be considered as 2 different superimposed emissions a and b without fundamentals.

waves are observed. Therefore peaks in a direction perpendicular to the magnetic field are observed that can provide free energy for wave growth. Let us now investigate in detail these correlations between wave occurrence and proton rings having $\partial f/\partial v_{\perp} > 0$.

3.2. Relationships Between ULF Waves and Proton Rings

The S-310 and S-321 proton data measured during July and August 1977 on board GEOS 1 have been systematically examined. This analysis has led to select some events corresponding to simultaneous detection of ULF waves and typical distribution functions of energetic protons. These selected events were observed on the dayside of the magnetosphere (mostly around 12 MLT) at radial distances greater than $5\,R_E$.

In Figure 11, data are shown corresponding to the July 1, 1977, event. The energy distribution between 300 eV and ~ 5 keV approximately fits with an exponentially decreasing function with intense fluxes $(10^6-10^7 \text{ cm}^{-2} \text{ sr}^{-1} \text{ s}^{-1} \text{. keV}^{-2})$. This is characteristic of the spectra observed by GEOS 1 in the equatorial plane of the magnetosphere [Borg et al., 1978]. At higher energies, a peak around 7 keV is detected. As evidenced by the middle panel of this figure, this peak is not only energy dependent, but it also depends upon the pitch angle. The largest maximum is for pitch angle close to 90° and a limited energy range. This is confirmed by the right panel where two distinct peaks are clearly visualized: one for $U_{\perp} \sim 1250$ km/s and the second at $U_{\perp} \sim 1850$ km/s. Owing to their particular shape, these peaks will be referenced to as rings in the perpendicular direction $(\partial f/\partial v_{\perp} > 0$ for small parallel velocities). Notice that in the present case there is also an almost empty loss cone.

The proton density in the ring (n_r) was computed by using a standard method: the numerical computation of the zero order moment of the distribution function f(v): $n_r = \int f(v) d^3 v$. Therefore one has to integrate the two-dimensional experimental function over the pitch angle and the energy around the peak, and assuming azimuthal symmetry.

In this example one obtains a high value of the density $n_r \approx 1.6 \text{ cm}^{-3}$ around 7 keV.

At the same time, harmonic emissions are detected in the ULF range. The fundamental f_1 is equal to 1.8 F_{H^+} and the first harmonic is clearly seen. The second one is not well defined. The amplitude at f_1 is 10 m γ .

In Figures 12a and 12b, two successive sequences within a time lag of 27 min are displayed. The first measurements were obtained around 1335 MLT, at $\lambda m \approx -6^{\circ}$ (figure 12a). In this sequence a ring of trapped protons around 18 keV is superimposed to the monotonic decreasing component, which is always observed. The pitch angle distribution is strongly anisotropic in the plane perpendicular to \mathbf{B}_0 . The loss cone is depleted as it is often observed on board GEOS 1

[Borg et al., 1978]. The ring density is $\sim 0.6 \text{ cm}^{-3}$ around 18 keV. At the same time an emission is observed in the ULF range at f=9.4 Hz, i.e., around $4F_{H^+}$. For this event, which occurred at a round hour in universal time, we had the opportunity to analyze the waves in the ELF range and the results have been presented on Figure 6. Up to fifth harmonics are detected in addition to f_1 . Besides, two other fundamentals ($f_2=11.65$ Hz and $f_3=13.25$ Hz) with their harmonics appear, as well as combination of these frequencies.

Twenty-seven minutes later (Figure 12b), the peak at 18 keV has completely disappeared. The energy spectrum has a monotonic behavior. The ULF waves have also disappeared.

During these two events (July 1 and 2, 1977) there are no proton data available from S-321 experiment.

A last example is given Figure 13. Data obtained simultaneously by S-310 and S-321 have been merged together. It is worth noticing that the absolute values of f(v) deduced from the two different experiments well agree in the intermediate energy range around 20 keV. A ring around 12 keV is again observed on the energy spectrum, with a maximum at 90° pitch angle. At higher energy, f(v) is always monotonous without any peak, only an empty loss cone is observed. The magnetosonic waves detected during this period show a complex spectrum, which consists of two different series of emissions: a_n and b_m .

These comparisons between energetic protons and ULF waves are summarized in Table 1, together with Figures 11, 12, and 13. They lead to the conclusion that when the proton distribution f(v) has a peak in the direction perpendicular to the magnetic field (which corresponds to a ring by symmetry around B_0) for a perpendicular velocity U_{\perp} larger than the Alfven energy, magnetosonic waves are generally detected. Such a connection between the proton distribution function and magnetosonic waves supports the interpretation, given in the next section, concerning the origin of these waves. The energies of the particles that are involved in these three cases are below 25 keV. Experiment S-321 shows a monotone decrease in the spectrum. Therefore the energy range of S-310 experiment seems to be more suitable for these studies. However, there are no continuous data sequences with a good pitch angle coverage. This has greatly limited detailed investigation of wave-particle correlation. For this reason the wave events presented in this section are somewhat less impressive than those shown in the previous section. It is also worth recalling at this point that MSW's are more commonly observed on GEOS 2 than on GEOS 1. This is because the former is close to the magnetic equator when MSW's take place, while the latter spent most of its trajectory outside of the region where MSW's are detected. Therefore most of the MSW's events displayed here were recorded on GEOS 2. Unfortunately, GEOS 2 data from the S-310 experiment are not presently available. It is clear that

TABLE 1. Characteristic Values of the Ring Distributions and Plasma Parameters Measured During Magnetosonic Events Observed in the Month of July 1977

Date	Hour, UT	L	λ _m (°)	Β, γ	$N_{\rm tot}$, cm ⁻³	$mV_A^2/2$, keV	cm^{-3}	E_r , ke ${ m V}$	ρ	U_{\perp}/V_{A}
July 1, 1977	11.16	6.25	-4	134	65	0.69	1.6	7.1	0.02	3.2
July 2, 1977	11.02	5.68	-6	158	9	6.9	0.6	20	0.07	1.7
July 28, 1977	11.12	6.1	4	146	80	0.66	0.17	12	0.002	4.3

a wave particle comparison based on GEOS 2 data would be much better

These ringlike distribution functions for the protons were not systematically observed when magnetosonic waves were detected. One must first notice that when a ring is observed as shown above, a loss cone distribution along \mathbf{B}_0 ($v_\perp \approx 0$) is sometimes also observed that could also provide a free energy for magnetosonic waves. However, we have not found any wave event during which a loss cone was observed without a ring.

Second, another kind of correlation between proton data and harmonically related emissions has been found: a sudden increase in the particle flux at 90° pitch angle often corresponds to a sudden commencement of a magnetosonic wave event [see *Perraut et al.*, 1978, Figure 10]. A detailed analysis of these events show that they correspond to sharp gradients in the spatial distribution of energetic protons. Such kinds of distribution are likely to occur in the dayside of the magnetosphere because of shell splitting effects induced by magnetic drift on particles that are freshly injected in the nightside during substorms. This last type of events will be studied in detail elsewhere.

4. DISCUSSION AND COMPARISON WITH THEORETICAL MODELS

In section 2 it has been shown that ULF waves that are observed above the proton gyrofrequency in the vicinity of the equator can be regarded as magnetosonic waves. On the other hand, in section 3 it has been shown that one possible free energy source that can account for the generation of these waves consists of ringlike distributions of energetic protons. Motivated by these observations we have developed a simple theoretical model for magnetosonic waves generation that includes a cold plasma plus a ringlike distribution characterized by

$$f = \frac{n_r}{2\pi v_\perp} \delta(V_{\parallel}) \delta(V_\perp - U_\perp) + \frac{N_c}{2\pi V_\perp} \delta(V_{\parallel}) \delta(V_\perp) \qquad (1)$$

where n_r and N_c are the ring and cold plasma densities, respectively, and U_{\perp} is the ring velocity in the perpendicular direction. It is important to emphasize that the instability that is investigated here is basically a hydromagnetic instability, since it still operates when $k_{\parallel} = 0$. Accordingly, the growth rate depends on the beam density rather than on the slope $\partial f/\partial v_{\perp}$ as it would have had for a kinetic instability. Of course, for a small but finite k_{\parallel} and a smoother distribution of protons one has in principle to take care of both effects in order to determine the exact numerical value of the growth rate. Since the hydromagnetic growth rate is proportional to $\sqrt{n_r}$ (the ring density), its contribution is generally dominant. Thus the present model is certainly oversimplified. Yet, as will be shown later it shed some light upon the connection between the observed magnetosonic waves and the energetic proton distribution. We have shown in part 2 that the waves are characterized by an ac magnetic field strongly aligned with the dc magnetic field B_0 , therefore demonstrating that the wave normal component parallel to \mathbf{B}_0 , $k_{||}$ must be very small. Then the precise shape of the proton distribution is not important because the instability is hydromagnetic. Let us notice that if k_{\parallel} was not much smaller than k_{\perp} the waves would be strongly damped by the main body of the proton distribution (ring excluded); this will be discussed at the end of this section. Before going into the

detail of the calculations let us mention that similar calculations with a less singular distribution function (a loss cone one) were performed by Gul'elmi et al. [1975]. However, these authors have used an analytical model that is not valid for frequencies on the order of the proton gyrofrequency, as is generally observed. Therefore, we have been obliged to use a more complete dispersion relation that can only be solved by numerical methods. Conversely, our calculations are limited to normalized frequencies $X = f/F_{H^+}$ smaller than ~10. This is sufficient for most of the comparisons discussed here, since the ULF experiment, for which data are systematically displayed, has a frequency range limited to 11.6 Hz. In some cases, such as the one displayed on Figure 6, we have performed a special analysis of the ELF range. Since magnetosonic waves were found to extend up to frequencies $f \approx 50$ Hz (with much smaller amplitudes, however), our calculations must be completed by those of Gul'elmi et al. [1975] as far as these ELF magnetosonic emissions are concerned.

It is worth mentioning that other authors have tried to interpret the origin of the waves discovered by Russell et al. [1970] and Gurnett [1976]. Curtis and Wu [1979] have shown that relativistic effects can induce resonances even when k_{\parallel} = 0, therefore leading to an imaginary dispersion relation and consequently to instabilities. Although protons do not need in such a theory to be highly relativistic ($E \sim 1$ MeV is sufficient for exciting fast magnetosonic waves), our results show that these waves are associated with protons of much lower energies whose fluxes are far more important. It is difficult to comment on the results of the other authors who found that MSW's can be excited by anti-loss cone distributions [Bhatia and Lakhina, 1980a] as well as by loss cone distributions [Bhatia and Lakhina, 1980b].

4.1. Computation of the Growth Rate

The distribution function given in (1) has been used for the calculation of the integrals in the general expressions of the determinant of the dispersion relation given by *Krall and Trivelpiece* [1973], for the Vlasov theory of small amplitude waves in an uniformly magnetized plasma.

The different terms of the determinant become

$$D_{xx} = \frac{1}{y^2} + \frac{1}{m} + \frac{1 - \rho}{1 - s^2} + \frac{\rho}{x} + \sum_{-n}^{+n} \frac{1}{\lambda} \frac{n^2}{n - x} J_n (J_{n-1} - J_{n+1})$$
 (2)

$$D_{yy} = \frac{1}{y^2} + \frac{1}{m} + \frac{1 - \rho}{1 - x^2} + \frac{\rho}{x} \sum_{-n}^{+n} \frac{1}{n - x}$$

$$\left|\frac{1}{2}\left(J_{n-1}-J_{n+1}\right)^{2}+\frac{\lambda}{4}\left(J_{n-1}-J_{n+1}\right)\left(J_{n+2}+J_{n-2}-2J_{n}\right)\right|$$
(3)

$$D_{xy} = -D_{yx}$$

$$D_{xy} = i \left\{ \frac{1}{x} - \frac{1 - \rho}{x(1 - x^2)} + \frac{\rho}{x} \sum_{-n}^{+n} \frac{n}{n - x} \right\}$$

$$\cdot \left[\frac{J_n}{2\lambda} (J_{n-1} - J_{n+1}) + \left(\frac{J_{n-1} - J_{n+1}}{4} \right)^2 + \frac{J_n}{4} (J_{n+2} + J_{n-2} - 2J_n) \right]$$
(4)

Where the parameters introduced in these expressions are

 $\lambda = k_{\perp} U_{\perp}/\Omega_{\rm H^+};$

 $Y = \omega_{pi}/\Omega_{H^+} = C/V_A$, where ω_{pi} is the proton plasma pulsation and V_A is the Alfven velocity;

 $\rho = n_r/N_{\text{tot}}$ is the ring density normalized to the total (cold plus hot) proton density;

m the ratio of the proton and electron masses;

 J_n the Bessel function of order n.

The instability being assumed to be hydromagnetic, the dispersion relation becomes simple:

$$D_{xx}\cdot D_{yy}-D_{xy}^2=0$$

In order to solve this equation we assume that X is complex and $k = k_{\perp}$ real. Thus

$$X = X_r + iX_i$$

The real part of X, X, gives the frequency of the emission, whereas the imaginary part X_i gives the growth rate.

In order to achieve the computations, we must fix the parameters. This is done by assuming a range of variation of ρ and U_{\perp}/V_A that is deduced from the measurements. In Table 1, three events that occurred during the month of July 1977 have been selected and the measured parameters are given. One sees that ρ varies between 2×10^{-3} and 7×10^{-2} , whereas U_{\perp}/V_A varies between 1.7 and 4.3. The computations have therefore been made for values of ρ and U_{\perp}/V_A situated in this range. Three examples are presented on Figures 14–16.

All examples show that the real part of the dispersion

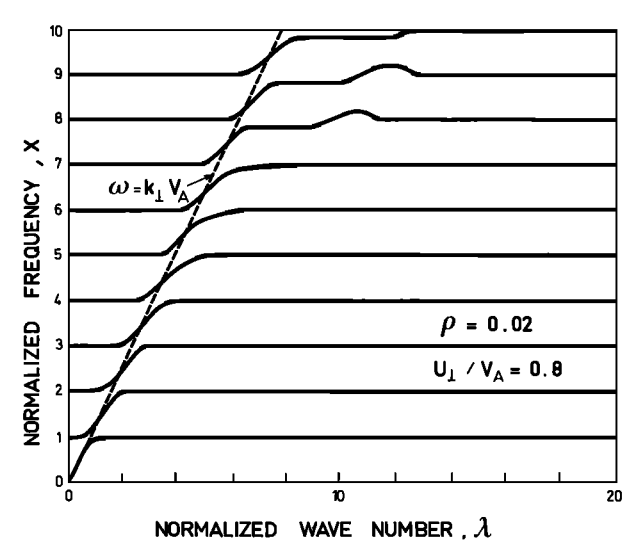
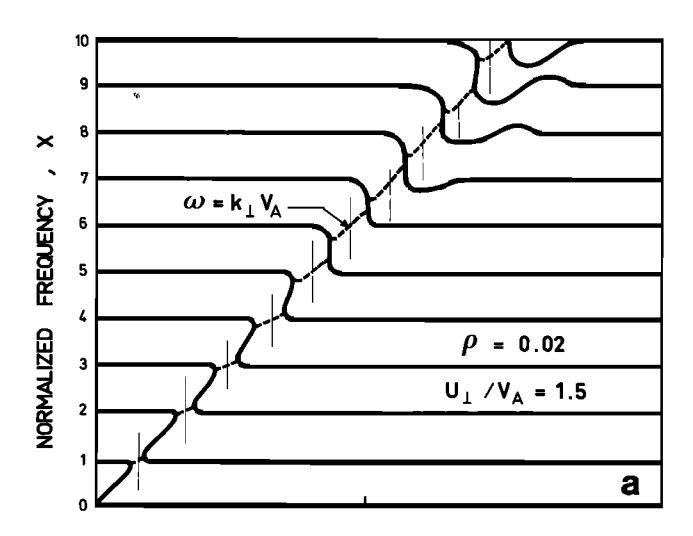


Fig. 14. Dispersion relation for magnetosonic waves propagating perpendicular to the magnetic field in a cold plasma (electrons and protons) containing a ringlike distribution of energetic protons with a relative density $\rho=2\%$. The ring velocity U_{\perp} is smaller than the Alfven velocity V_A , $(U_{\perp}/V_A=0.8)$. The cold plasma dispersion relation $\omega=k_{\perp}V_A$ is drawn (dashed line). The growth rates γ deduced from the computation are very small ($<10^{-12}$) in this case and are not represented.



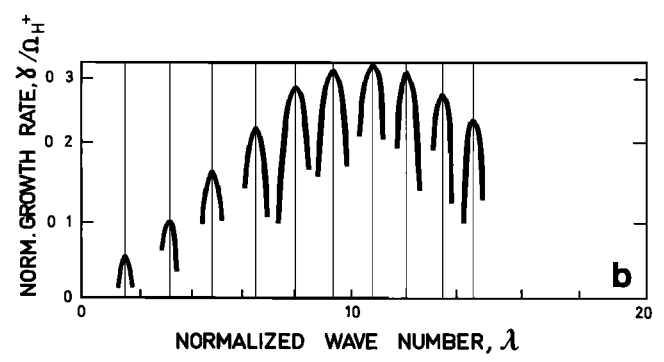
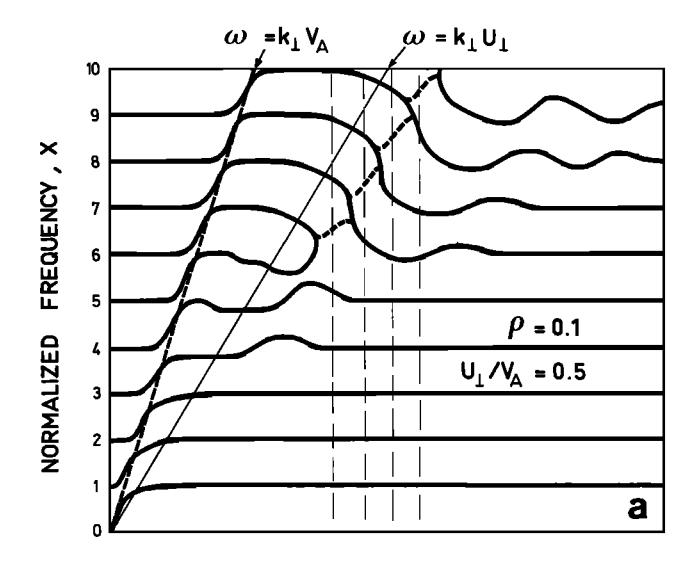


Fig. 15. (a) Same as Figure 14, but $U_{\perp}/V_A=1.5$. (b) The normalized growth rate γ/Ω_H^+ is plotted as a function of $\lambda=k_{\perp}U_{\perp}/\Omega_{H^+}$. The growth rate γ is only large in regions where the dispersion relation has complex conjugate roots (dashed portions). It peaks for different values of λ corresponding to the intersection between the different horizontal branches ($\omega=n\Omega_{H^+}$, i.e., X=n) and the dispersion curve $\omega=k_{\perp}V_A$ for the cold magnetosonic mode.

relation is characterized by multiple branches. In each of these branches $\omega \sim n\Omega_{\rm H^+}$ except in the close vicinity of the cold plasma dispersion curve where the frequency is single valued and is linked to the wave number by $\omega \sim k_{\perp} V_a$ (the cold plasma dispersion relation). These branches may join monotonically (Figure 14) from $\omega = n\Omega_{H^+}$ to $\omega = (n+1)\Omega_{H^+}$. In this case the dispersion curves resemble the ones that are valid for extraordinary ULF waves propagating with $k_{\parallel} = 0$ in a thermal plasma [see Curtis and Wu, 1979, Figure 2]. There is no instability, the interaction being nonresonant and the dispersion equation being real. In other regions of the ω , k_{\perp} plane (upper part of Figure 16, or Figure 15), there are ranges of k_{\perp} for which the real dispersion relation has only complex roots; these are the regions of non resonant instability. A similar situation was shown to occur for perpendicularily propagating electron cyclotron harmonic waves in the presence of ring distributions [Tararonis and Crawford, 1970].

As far as growth rates are concerned, two cases must be considered. For rings of weak densities ($\rho \sim 0.02$) the computations show that the growth rate γ is positive only when the average velocity of the ring is larger than the Alfven velocity ($U_{\perp}/V_A > 1$). It is maximum at the crossing points of the cold plasma dispersion curve ($\omega = k_{\perp} V_A$) and the 'ringlike' solutions ($\omega = n\Omega_{\rm H^+}$). The growth rate increases with n, which may explain why sometimes only the



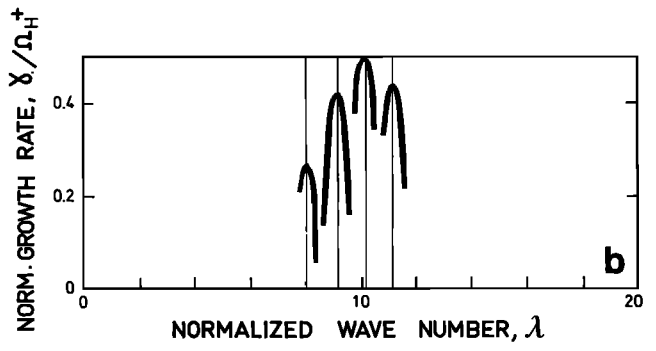


Fig. 16. Same as Figure 14, but with a strong ringlike distribution of protons ($\rho=10\%$) and with $U_{\perp}/V_A=0.5$. Important growth rates are observed although $U_{\perp}/V_A<1$.

higher harmonics are observed (Figure 3). For large values of n (n=8 in Figure 15), γ seems to decrease when n increases. In fact, when U_{\perp}/V_A is large the envelope of the growth rate is oscillating. These oscillation reflect interferences between the zeroes of the Bessel function. We consider them as unphysical because they would not appear with smooth distribution functions.

For more intense rings ($\rho \sim 0.1$, Figure 16), the relations $U_{\perp}/V_A > 1$ is no more a condition for the medium to be unstable. A jump in the dispersion branches from the *n*th to the (n+1)th gyroharmonic still occurs at $\omega = k_{\perp}V_A$, but waves are unstable in some of the regions where $n\Omega_{H^+} = k_{\perp}U_{\perp}$. The number of gyroharmonics excited in this case is much less than in the previous cases.

This change in the generation conditions fits with experimental observations. In the nighttime, U_\perp/V_A is lower than in the dayside since V_A is larger, but ρ is rather large because in the injection region n_r is large, whereas the cold plasma density N_c is small. Therefore there is no restriction on the U_\perp/V_A ratio. In the dusk and dayside region $\rho=n_r/N_c$ has much decreased so that one must have $U_\perp/V_A>1$, which is easily satisfied as a consequence of the large increase of N_c . On the morningside, on the other hand, only low energy (\lesssim 5 keV) protons can be brought there by the global convection plus corotation mechanism and U_\perp/V_A is not sufficiently large to allow MSW's to be generated.

4.2. Harmonicity of the Emissions

As emphasized earlier, most of the observed magnetosonic waves have spectra that are characterized by an harmonic structure. Growth rate calculations performed here as well as those performed by $Gul'elmi\ et\ al.$ [1975] lead to the conclusion that wave growth is limited to the near vicinity of the various gyroharmonics (at least for a weak ring). Many observed events do present such a structure. However, as emphasized in part 2, some events have a fundamental frequency that is not close to $F_{\rm H^+}$ but still exhibits a clear harmonic structure. For instance one can have $F_1 \simeq 1.5\ F_{\rm H^+},\ F_2 \simeq 3\ F_{\rm H^+}$, etc. Such a frequency spectrum cannot be described a priori by the present calculations. There are three possible interpretations for this effect.

- 1. One likely possibility is that magnetosonic waves are, in their source region, generated at $F_n \simeq nF_{\rm H^+}$ and then while propagating inward or outward penetrate in regions where $F_{\rm H^+}$ is different; accordingly, their normalized frequencies vary, thus explaining why locally $F_n \neq nF_{\rm H^+}$. The interesting aspect of this interpretation is that one obtains harmonically related waves everywhere because they had an harmonic structure in their source region. This model is illustrated in Figure 17. However, with such a model we should expect to have the largest amplitudes in the source region, that is when $F \sim nF_{\rm H^+}$ (provided that the wave propagates radially. This is not always observed.
- 2. A second possibility is that the hypothesis used in the calculations namely that $k_{||}=0$ is not valid and that the instability is due to a loss cone distribution (the ring being just the limit of this loss cone type distribution). Then the instability becomes kinetic and the resonance condition: $\omega k_{||}V_{||} = n\Omega_{H^+}$ is now compatible with $\omega \neq n\Omega_{H^+}$. Nevertheless, such a model cannot account for the harmonicity in the observed spectra because it would lead to $\omega_n \omega_{n-1} \simeq \Omega_{H^+}$ instead of the observed harmonic structure.

It is also worth mentioning that magnetosonic waves corresponding to k_{\parallel}/k_{\perp} not much smaller than unity (as required in order to provide an interpretation of the shift $\Delta\omega = \omega - n\Omega_{\rm H^+}$) would be strongly damped by lower energy protons ($E_{\rm th} \sim 2$ keV) which are observed to be generally isotropic (see figures in section 3).

Incidentally, such an absorption effect, not taken into account in the computations leading to Figure 14 to 16, could be at the origin of the events for which the first harmonics

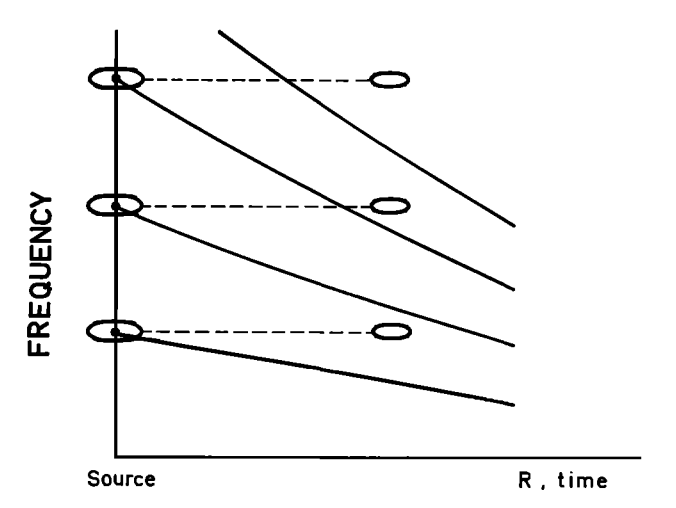


Fig. 17. Radial propagation of MSWs. One assumes that in the source region, harmonic emissions with a fundamental in the close vicinity of the local $F_{\rm H^+}$ can be generated. These waves with ${\bf k_\perp B_0}$ can radially propagate in other regions where the fundamental differs from the local $F_{\rm H^+}$; the harmonic character of the emission is conserved.

are not detected (Figure 3). The growth rate due to the energetic and anisotropic part of the distribution function exceeds the damping due to the less energetic but isotropic part, only for the higher harmonics.

3. A third possibility is that the harmonic structure has a nonlinear origin; for instance, the second harmonic could be generated by beatings between two waves at the 'fundamental' frequency. For such an interpretation to be valid it is necessary that the fundamental has the largest energy level, which is generally observed but is somehow contradicted by the fact that the linear growth rate increases as the order of the harmonic increases.

It is difficult to test this last interpretation a priori since, as said above, the observed harmonic structure can be explained by (1) as well as by (3). Nevertheless, in some cases one can prove that the shape of the spectrum is determined by nonlinear effects. (This has been discussed in section 2.3 and illustrated by Figures 6 and 8. This cannot be interpreted by (1) and thus clearly points out at a nonlinear origin for the observed structure, as the one suggested in (3). Therefore sometimes, if not always, the observed harmonic structure of the spectrum seems to be related to nonlinear effects. This is not surprising, even with moderate amplitudes, since unstable waves lie on or close to the dispersion relation $\omega = k_{\perp}V_A$, a 'linear' relation that favors strong mode-mode coupling. In other words, the necessary conditions for mode coupling

$$D(\omega_i, k_i) = 0$$

$$\mathbf{k}_1 + \mathbf{k}_2 = \mathbf{k}_3$$

$$\omega_1 + \omega_2 = \omega_3$$

are automatically satisfied provided that $k_{||i|} \simeq 0$ and $\omega_i/k_{\perp i} \simeq V_A$.

5. Conclusion

Because of its high sensitivity and good frequency resolution, the ULF experiment onboard GEOS has allowed for a detailed study of a type of quasi-monochromatic emissions occurring in the vicinity of the geostationary orbit and that were previously mentioned to exist at lower radial distances [Russell et al., 1979; Gurnett, 1976]. These emissions have a long duration (up to 5 hours) and intensities ranging from ~ 30 to $200 \text{ m}\gamma$. They are characterized by their polarization and their frequency structure.

Contrary to other ULF emissions observed in this frequency range [Perraut et al., 1978; Young et al., 1981] these waves are mainly polarized along the dc magnetic field \mathbf{B}_0 , implying a propagation vector almost orthogonal to it. The ratio of the magnetic component parallel to \mathbf{B}_0 to the components perpendicular to it is high (~ 20 -30 dB). When they are observable, the circular components of these waves are right handed. When simultaneous measurements with the GEOS electric antenna are available, these measurements show that the ratio E/B is of the order of the Alfven velocity. Therefore these waves have been identified as magnetosonic waves (MSW) propagating in a direction almost perpendicular to \mathbf{B}_0 ; they are likely to propagate radially, but detailed ray tracing of MSW's that are presently under progress are necessary to assess this point.

These waves do have a well-defined harmonic structure. The number of harmonics is high (up to 8 harmonics have been observed) so that their frequencies often exceed the frequency range of the ULF experiment (11.6 Hz). In one

occasion when the GEOS ELF experiment was operated in a suitable mode, emissions up to 50 Hz have been observed. The fundamental frequency of the emission generally lies in the vicinity of the local proton gyrofrequency, but this is not always the case. If an event contains more than one fundamental frequency, nonlinear coupling between the different harmonics often occurs.

The MSW's are strongly confined in the equatorial region (within \pm 10°) and at all radial distances explored by GEOS 1 (4 $\leq R/R_E \lesssim$ 8). They are a rather common phenomenon at the geostationary altitude (GEOS 2), the probability of detecting such an event within a given hour is approximately at an average of 12% and reaches 50% near noon or midnight. MSW's are often observed within the plasmasphere, but they have also been observed outside the plasma pause in the night sector.

Complete distribution functions of low (<20 keV) and medium (>20 keV) energy protons, as deduced from two particle experiments onboard GEOS [Borg et al., 1978; Korth et al., 1978] have been drawn for some events. Examination of these distribution functions shows that when a peak exists in the energy spectra and when this peak is more pronounced for 90° pitch angle (a ringlike distribution function for $v_{\parallel} \approx 0$), MSW's are simultaneously observed.

A simple model has been used to compute in the hydromagnetic limit (flute mode) the stability of such ringlike distribution functions. This model extends to frequencies closer to the proton gyrofrequency than previous calculations made by Gul'elmi et al. [1975]. It accounts for most of the observed characteristics of MSW's. Indeed MSW's are destabilized when the perpendicular velocity of the ring U_{\perp} exceeds the Alfven velocity; it also predicts the observed polarization and frequency structure, $F \approx nF_{H^+}$. However, the latter characteristic ($F = nF_{H^+}$) is not always observed, which can apparently be explained by radial propagation of MSWs. Furthermore some of MSW's characteristics clearly indicate that strong nonlinear mode-mode coupling are operating. This is not surprising since the dispersion relation of unstable wave is roughly given by $\omega = k_{\perp}V_A$, which indeed favors nonlinear effects. The saturation mechanism of the flute instability remains to be investigated. It is suggested that during their propagation MSW's get a small k_{\parallel} . Then they are likely to be cyclotron damped by the main body of the proton distribution function. According to this tentative interpretation the free energy in the ring (5 < E < 20 keV)would be transferred through MSW's to the low-energy protons (0.1 < E < 5 keV).

Acknowledgments. We wish to thank M. Avignon of CNES, M. Parrot of CRPE Orléans, B. de la Porte des Vaux of CRPE Issy, G. Giordano of CESR, and H. J. Müller, F. Both, and J. Wallbrecht of MPA Lindau for their contributions to the large amount of data analysis used in this study. We thank S-301 and S-304 experimenters J. Etcheto, P. Decreau, and B. Higel for providing electron density data, the S-310 experimenters B. Hultqvist and H. Borg for low energetic particle data, and the S-331 experimenters for magnetometer data. Early discussions with D. Jones are acknowledged. Work at MPA Lindau was supported by the Max-Planck-Gesellschaft für Forschung und Technologie through DFVLR-PT under contract RV 14-B 12/73 (WRK 243)—SF 21.

The Editor thanks S. P. Gary and C. T. Russell for their assistance in evaluating this paper.

REFERENCES

Ashour-Abdalla, M., and S. W. H. Cowley, Wave-particle interactions near the geostationary orbit, in *Magnetospheric Physics*,

- edited by B. M. Mc Cormac, pp. 241-270, D. Reidel, Hingham, Mass., 1974.
- Ashour-Abdalla, M., and C. F. Kennel, Nonconvective and convective electron cyclotron harmonic instabilities, J. Geophys. Res., 83, 1531-1543, 1978.
- Ashour-Abdalla, M., J. N. Leboeuf, J. M. Dawson, and C. F. Kennel, A simulation study of cold electron heating by loss cone instabilities, Geophys. Res. Lett., 7, 889-892, 1980.
- Balsiger, H., P. Eberhardt, J. Geiss, and D. T. Young, Magnetic storm injection of 0.9 to 16 keV/e solar and terrestrial ions into the high-altitude magnetosphere, J. Geophys. Res., 85, 1645–1662, 1980.
- Bhatia, K. G., and G. S. Lakhina, Instability near proton-cyclotron harmonics due to anti-loss cone proton distributions, *Astrophys. Space Sci.*, 68, 175–182, 1980a.
- Bhatia, K. G., and G. S. Lakhina, Proton-cyclotron instabilities in non-uniform loss-cone magnetospheric plasma, *Astrophys. Space Sci.*, 70, 467-481, 1980b.
- Borg, H., L.-A. Holmgren, B. Hultqvist, F. Cambou, H. Reme, A. Bahnsen, and G. Kremser, Some early results of the keV plasma experiment on GEOS-1, Space Sci. Rev., 22, 511-535, 1978.
- Borg, H., L. A. Holmgren, B. Hultquist, S. Olsen, A. Bahnsen, S. Laursen, F. Cambou, H. Reme, and G. Kremser, The keV plasma experiment on the GEOS-1 and GEOS-2 satellites, Space Sci. Instrum., 5, 37-49, 1979.
- Christiansen, P. J., M. P. Gough, G. Martelli, J. J. Bloch, N. Cornilleau, J. Etcheto, R. Gendrin, C. Beghin, P. Decreau, and D. Jones, GEOS-1 observations of electrostatic waves, and their relationship with plasma parameters, Space Sci. Rev., 22, 383-400, 1978.
- Cornilleau-Wehrlin, N., A new ULF-modulated electrostatic wave detected in the extremely low frequency range onboard GEOS, J. Geophys. Res., 86, 1365-1373, 1981.
- Curtis, S. A., and C. S. Wu, Gyroharmonic emissions induced by energetic ions in the equatorial plasmasphere, J. Geophys. Res., 84, 2597-2607, 1979.
- Fredricks, R. W., and F. L. Scarf, Recent studies of magnetospheric electric field emissions above the electron gyrofrequency, J. Geophys. Res., 78, 310-314, 1973.
 Galperin, Y. I., N. V. Jorjio, R. A. Kovrazhkin, F. Cambou, J. A.
- Galperin, Y. I., N. V. Jorjio, R. A. Kovrazhkin, F. Cambou, J. A. Sauvaud, and J. Crasnier, On the origin of auroral protons at the dayside auroral oval, Ann. Geophys., 32, 117-129, 1976.
- Gendrin, R., Some aspects of ULF waves observed onboard GEOS related to convection, heating and precipitation processes, in *Exploration of the Polar Upper Atmosphere*, edited by C. S. Deehr and J. A. Holtet, pp. 337-354, D. Reidel, Hingham, Mass., 1980.
- Gendrin, R., S. Perraut, H. Fargetton, F. Glangeaud, and J. L. Lacoume, ULF waves: Conjugated ground-satellite relationships, Space Sci. Rev., 22, 433-442, 1978.
- Gough, M. P., P. J. Christiansen, G. Martelli, and E. J. Gershuny, Interaction of electrostatic waves with warm electrons at the geomagnetic equator, *Nature*, 279, 515-517, 1979.
- Gul'elmi, A. V., B. I. Klaine, and A. S. Potapov, Excitation of magnetosonic waves with discrete spectrum in the equatorial vicinity of the plasmapause, *Planet. Space Sci.*, 23, 279-286, 1975.
- Gurnett, D. A., Plasma wave interactions with energetic ions near the magnetic equator, J. Geophys. Res., 81, 2765-2770, 1976.
- Higel, B., and W. Lei, Geosynchronous electron density and plasmapause characteristics: First statistical studies from the measurements of the GEOS 2 active wave relaxation sounder, submitted to J. Geophys. Res., 1982.
- Hubbard, R. F., and T. J. Birmingham, Electrostatic emissions between electron gyroharmonics in the outer magnetosphere, J. Geophys. Res., 83, 4837–4850, 1978.
- Hubbard, R. F., T. J. Birmingham, and E. W. Hones, Jr., Magneto-spheric electrostatic emissions and cold plasma densities, J. Geophys. Res., 84, 5828-5838, 1979.
- Kennel, C. F., F. L. Scarf, R. W. Fredricks, J. H. Mc Gehee, and F. V. Coroniti, VLF electric field observations in the magnetosphere, J. Geophys. Res., 75, 6136-6152, 1970.
- Kivelson, M. G., and D. J. Southwood, Local time variations of particle flux produced by an electrostatic field in the magnetosphere, J. Geophys. Res., 80, 56-65, 1975.
- Knott, K., Payload of the 'GEOS' scientific geostationary satellite, ESA Sci. Tech. Rev., 1, 173-196, 1975.

- Kodera, K., R. Gendrin, and C. de Villedary, Complex representation of a polarized signal and its application to the analysis of ULF waves, J. Geophys. Res., 82, 1245-1255, 1977.
- Konradi, A., D. J. Williams, and T. A. Fritz, Energy spectra and pitch angle distributions of storm time and substorm-injected protons, *J. Geophys. Res.*, 78, 4739-4744, 1973.
- Korth, A., G. Kremser, and B. Wilken, Observations of substorm-associated particle-flux variations at $6 \le L \le 8$ with GEOS-1, Space Sci. Rev., 22, 501-509, 1978.
- Krall, N., and A. Trivelpiece, Principles of Plasma-Physics, p. 405, McGraw-Hill, New York, 1973.
- Kurth, W. S., L. A. Frank, M. Ashour-Abdalla, D. A. Gurnett, and B. G. Burek, Observations of a free-energy source for intense electrostatic waves, *Geophys. Res. Lett.*, 7, 293-296, 1980.
- Mauk, B. H., and C. E. Mc Ilwain, Correlation of Kp with the substorm-injected plasma boundary, J. Geophys. Res., 79, 3193– 3196, 1974.
- Perraut, S., R. Gendrin, P. Robert, A. Roux, C. de Villedary, and D. Jones, ULF Waves observed with magnetic and electric sensors on GEOS-1, Space Sci. Rev., 22, 347-369, 1978.
- Robert, P., K. Kodera, S. Perraut, R. Gendrin, and C. de Villedary, Amplitude et polarisation des ondes UBF détectées à bord du satellite GEOS-1: Méthode d'analyse, problèmes rencontrés et solutions pratiques, Ann. Telecommun., 34, 179-186, 1979.
- Roederer, J. G., and E. W. Hones, Jr., Motion of magnetospheric particle clouds in a time-dependent electric field model, J. Geophys. Res., 79, 1432-1438, 1974.
- Rönmark, K., H. Borg, P. J. Christiansen, M. P. Gough, and D. Jones, Banded electron cyclotron harmonic instability: A first comparison of theory and experiment, Space Sci. Rev., 22, 401-417, 1978
- Russell, C. T., R. E. Holzer, and E. J. Smith, OGO 3 observations of ELF noise in the magnetosphere, 2, The nature of the equatorial noise, J. Geophys. Res., 75, 755-768, 1970.
- S-300 Experimenters, Measurements of electric and magnetic wave fields and of cold plasma parameters on-board GEOS-1: Preliminary results, *Planet. Space Sci.*, 27, 317–339, 1979.
- Sauvaud, J. A., J. Crasnier, K. Mouala, R. A. Kovrazhkin, and N. V. Jorjio, Morning sector ion precipitation following substorm injections, J. Geophys. Res., 86, 3430-3438, 1981.
- Shaw, R. R., and D. A. Gurnett, Electrostatic noise bands, associated with the electron gyrofrequency and plasma frequency in the outer magnetosphere, J. Geophys. Res., 80, 4259-4271, 1975.
- Smith, P. H., and R. A. Hoffman, Direct observations in the dusk hours of the characteristics of the storms time ring current particles during the beginning of magnetic storms, *J. Geophys. Res.*, 79, 966-971, 1974.
- Solomon, J., On the azimuthal drift of substorm-injected protons, J. Geophys. Res., 81, 3452-3454, 1976.
- Tataronis, J. A., and F. W. Crawford, Cyclotron harmonic wave propagation and instabilities, 1, Perpendicular propagation, J. Plasma Phys., 4, 231-248, 1970.
 Taylor, W. W. L., and L. R. Lyons, Simultaneous equatorial
- Taylor, W. W. L., and L. R. Lyons, Simultaneous equatorial observations of 1- to 30-Hz waves and pitch angle distributions of ring current ions, J. Geophys. Res., 81, 6177-6183, 1976.
- Taylor, W. W. L., B. K. Parady, and L. J. Cahill, Jr., Explorer-45 observations of 1- to 30-Hz magnetic fields near the plasmapause during magnetic storms, J. Geophys. Res., 80, 1271-1286, 1975.
- Winckler, J. R., The origin and distribution of energetic electrons in the Van Allen radiation belts, in *Particles and Fields in the Magnetosphere*, edited by B. M. McCormac, p. 332, D. Reidel, Hingham, Mass., 1970.
- Young, D. T., Ion composition measurements in mangetospheric modeling, in *Quantitative modeling of Magnetospheric Processes, Geophys. Monogr. Ser.*, vol. 21, edited by N. P. Olson, pp. 340-363, AGU, Washington, D. C., 1979.
- Young, D. T., S. Perraut, A. Roux, C. de Villedary, R. Gendrin, A. Korth, G. Kremser, and D. Jones, Wave-particle interactions near Ω_{He^+} observed on GEOS 1 and 2, 1, Propagation of ion cyclotron waves in He⁺ rich plasma, J. Geophys. Res., 86, 6755–6772, 1981.

(Received February 12, 1982; revised April 29, 1982; accepted April 30, 1982.)